# NASA Technical Memorandum 89164

# Nonlinear Shell Analyses of the SRB/ETA Ring Interface

Norman F. Knight, Jr.

July 1987

(NASA-TM-89164) NONLINEAR SHELL ANALYSES OF THE SRB/ETA RING INTERFACE (NASA) 62 p
Avail: NTIS HC A04/MF A01 CSCL 20K

N87-29883

Unclas
G3/39 0098985

National Aeronautics and Space Administration

**Langley Research Center**
Hampton, Virginia 23665

# NONLINEAR SHELL ANALYSES OF THE SRB/ETA RING INTERFACE

Norman F. Knight, Jr.†

## INTRODUCTION

The accident which destroyed the space shuttle Challenger is believed to have been caused by the failure of a case joint in the right solid rocket motor (SRM) aft attachment segment.[1] The upper end of a lower cylindrical, motor segment (e.g., aft attachment segment) forms a clevis. The lower end of an upper cylindrical, motor segment (e.g., aft center segment) forms a tang which mates with the lower clevis. Around the circumference of both tang and clevis ends are 180 holes into which one-inch-diameter connecting pins are inserted. Three of the pin holes on the tang end are used as alignment slots to facilitate assembly of the SRM segments. The seal between two motor segments is provided by two O-rings in the "inner arm" of the clevis. The O-rings are compressed by a flat sealing surface on the tang.

Several characteristics of the original SRM joint design have been identified as potential contributors to the failure. One characteristic is the behavior of the joint under internal pressure load. The motor case expands radially outward due to the pressure. Because the joint has a higher hoop stiffness than the case wall on either side of the joint, its radial expansion is less than that of the case wall. In addition to the nonuniform stiffness in the longitudinal direction due to the presence of the case joints, a nonuniform stiffness in the circumferential direction exists in the aft attachment segment due to the external tank attachment (ETA) ring. Nonuniform radial expansion is the primary cause of relative motion between the inner clevis arm and the sealing surface on the tang. This relative motion can cause the O-rings to become unseated and therefore lose their sealing capability.

Two-dimensional shell models of the portion of the solid rocket booster (SRB) with the ETA ring have been developed using the STAGSC-1 computer code. The purpose of these analyses is to calculate the overall deflection and stress distributions for the SRB/ETA ring interface.

† Aerospace Engineer, Structural Mechanics Branch, Structures and Dynamics Division.

# SRB/ETA RING INTERFACE

- OVERVIEW OF SRB/ETA RING GEOMETRY
- ANALYSIS METHOD AND FINITE ELEMENT MODELS
- NONLINEAR SHELL ANALYSES AND RESULTS

## SRB/ETA RING INTERFACE

The nonlinear shell analyses of the SRB/ETA ring interface are described in this paper. These analyses were performed in support of the SRB recertification program underway at the NASA Marshall Space Flight Center. An overview of the SRB/ETA ring geometry is presented followed by a discussion of the analysis method and finite element models. Finally, the nonlinear structural response of the SRB/ETA ring interface is discussed.

# OVERVIEW OF SRB/ETA RING INTERFACE

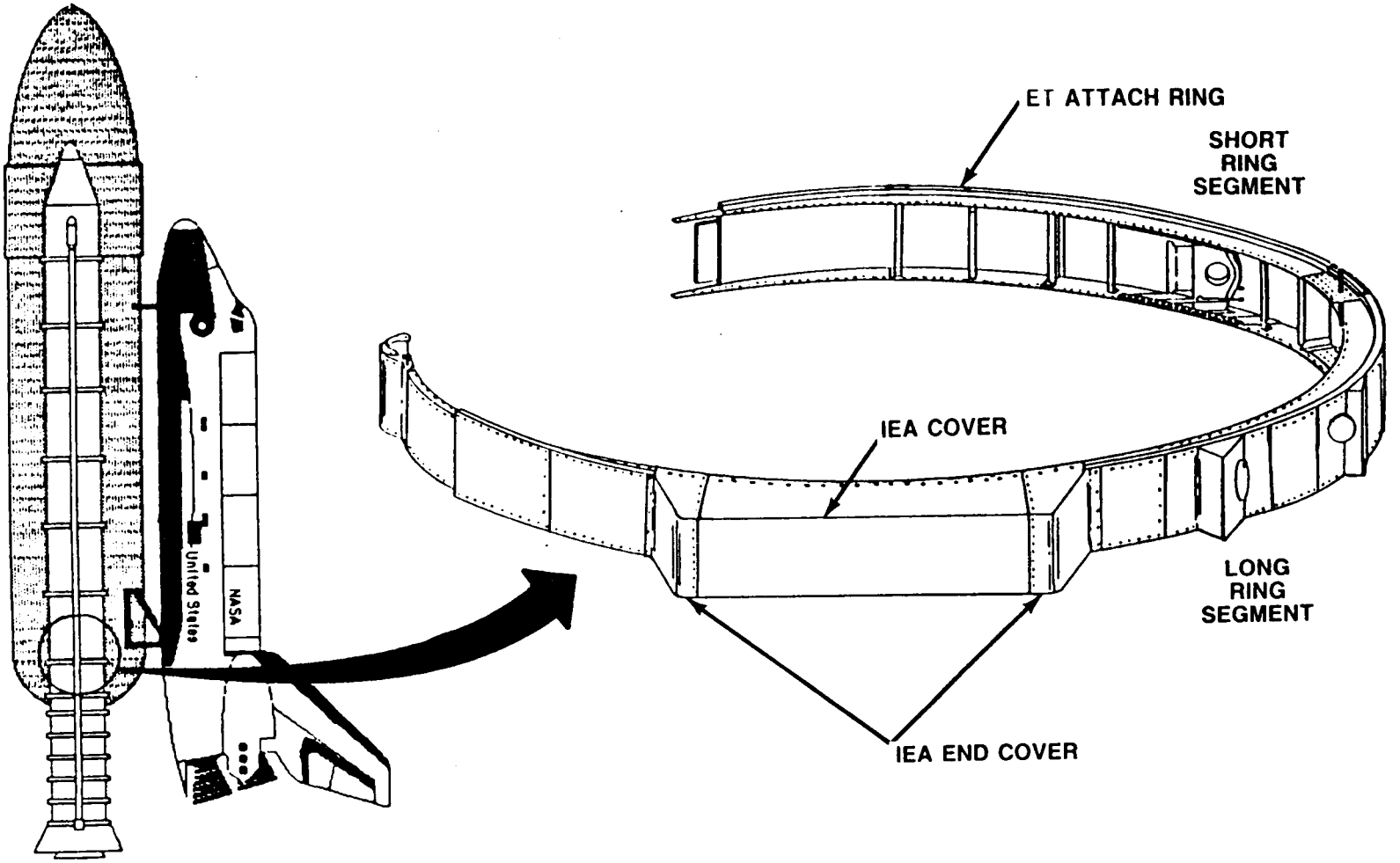

## OVERVIEW OF SRB/ETA RING INTERFACE

The SRB structural subsystem provides the necessary structural support for the shuttle vehicle on the launch pad, transfers thrust loads to the Orbiter and external tank (ET), and provides the housing, structural support and bracketry needed for the recovery system, the electrical components, the separation motors, and the thrust vector control system. This subsystem consists of the nose cone assembly, the forward skirt including the forward SRB/ET attach fitting, the aft SRB/ETA ring and struts, the aft skirt including the heat shield, the systems tunnel, and other structure for mounting other SRB subsystems components.

Each SRB is approximately 144 feet long. Nominal dimensions for the SRM case radius and thickness are 72.6 inches and 0.479 inches, respectively. These values correspond to a radius-to-thickness ratio of approximately 150. The rocket consists of several segments that are located along its length by station numbers that correspond to the x-coordinate of the SRB coordinate system. These segments include the aft center segment (station 1171.48 to 1491.48) and the aft attachment segment (station 1491.48 to 1823.85). The motor cases connected together by a tang-clevis joint are assembled at the launch site. These joints are referred to as "field joints". Field joints are located at stations 851.48, 1171.48, and 1491.48. Each of the upper three motor segments contain one additional tang-clevis joint that is assembled at the factory. These joints are referred to as "factory joints". The aft attachment segment has two of these factory joints (at stations 1577 and 1697).

The mechanical loading conditions for the SRB/ETA interface arise from the external tank (ET) attachment points and the SRM pressure load. The ET strut loads vary with time after the space shuttle main engine (SSME) ignition. The SRM internal pressure is 1000 psi; however, the pressure does vary longitudinally by approximately 100 psi along the entire length of the SRM.

# DEFINITION OF SRB/ETA RING INTERFACE

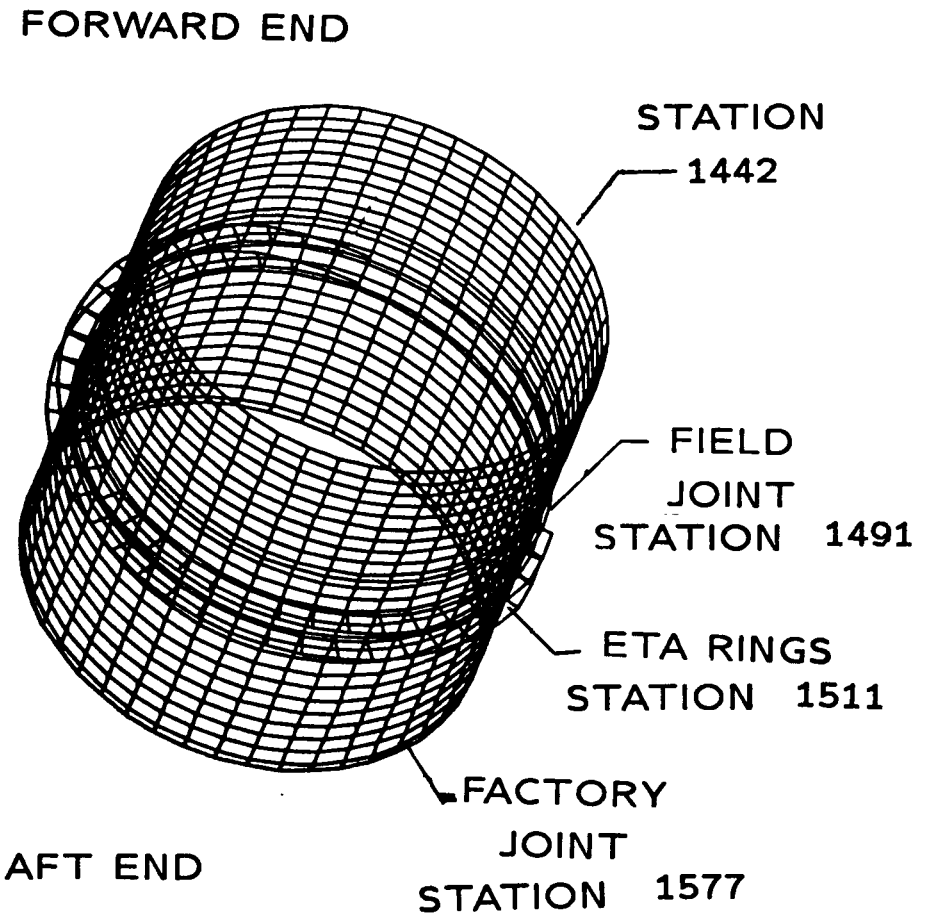


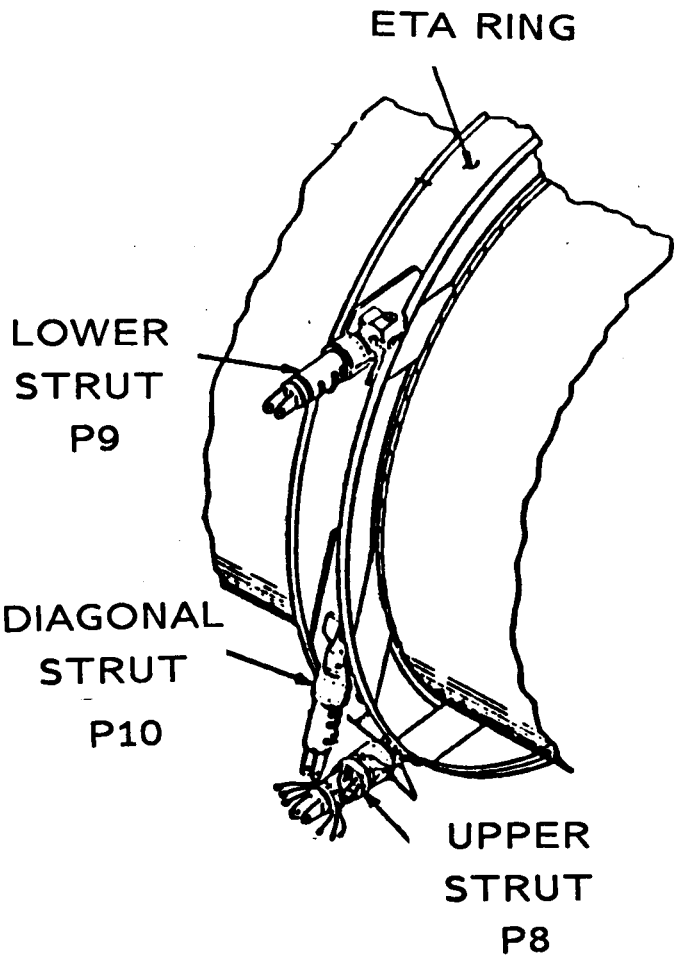

## DEFINITION OF SRB/ETA RING INTERFACE REGION

The definition of the SRB/ETA ring interface region for this paper includes both of the ETA rings (ring webs are approximately 12 inches apart), a portion of the SRM aft attachment segment including the factory joint at station 1577 (approximately sixty inches of shell), and a portion of the aft center segment including the field joint at station 1491 (approximately 64 inches of shell). The total length of the SRB/ETA ring interface region considered in this paper is 136 inches. This length corresponds roughly to one shell radius on either side of the ETA rings.

The center of the SRB/ETA ring interface region is located at station 1511, approximately twenty inches below the aft attachment segment field joint. The ETA ring assembly is comprised of two tapered, partial rings, H-fittings to attach the ET struts, cover plates, and various other intercostals and brackets. The ETA ring assembly extends only 270-degrees circumferentially around the SRM segment. The ETA rings are bolted every 2-degrees around the circumference to stub rings which are integral parts of the SRM aft attachment segment. Three struts attach the aft ends of the SRB and the ET. These three attachment struts are designated the lower strut (P9), the diagonal strut (P10), and the upper strut (P8).

# STRUCTURAL ANALYSIS OF GENERAL SHELLS (STAGSC-1)

- DEVELOPED BY LOCKHEED PALO ALTO (ALMROTH, BROGAN, STANLEY, RANKIN)
- 2-D FINITE ELEMENT ANALYSIS
- DISPLACEMENT FORMULATION
- MOUNTS (NONLINEAR SPRINGS), BEAMS, PLATES, SHELLS
- GEOMETRICALLY LINEAR OR NONLINEAR
- ELASTIC OR INELASTIC
- BUCKLING, COLLAPSE, VIBRATION, TRANSIENT DYNAMICS
- AVAILABLE AT COSMIC

## STRUCTURAL ANALYSIS OF GENERAL SHELLS
## - STAGSC-1 -

The STAGSC-1 computer code [2,3] has been under development for over 15 years and its development was initiated to support the design and analysis of the space shuttle system. The principal developers were Bo Almroth, Frank Brogan, Gary Stanley, and Charles Rankin of the Lockheed Palo Alto Research Laboratory. STAGSC-1 is a 2-D shell finite element analysis code based on the displacement formulation. The element library includes nonlinear spring or mount elements, 1-D beam elements, and 2-D plate/shell elements. Analysis options are provided for including geometric and material nonlinearities for buckling, collapse, vibration, or transient dynamic analysis. STAGSC-1 is supported on CDC, VAX, and CRAY computers and is available through COSMIC.

The modeling strategy used in the STAGSC-1 computer code involves the concepts of a shell unit and an element unit. A shell unit may be viewed as a substructure or superelement for the purpose of modeling convenience only. A shell unit may be composed of hundreds of nodes and elements, and automatic mesh generation facilities are provided for several common geometries for plate and shell structures. Mesh generation for a shell unit is accomplished by specifying the number of rows and columns of grid lines in each coordinate direction, not the number of elements. For example, a mesh with two rows and two columns represents one quadrilateral finite element. An element unit is perhaps more like conventional finite element codes in terms of required input data (e.g., node and element numbers, nodal coordinates, nodal connectivities) and provides the flexibility to model general shell-type structures. User-written subroutines are available for the user to write mesh generation utilities that meet specific needs.

# SRB/ETA RING INTERFACE FINITE ELEMENT MODELS

- ORIGINAL 51-L GEOMETRY
- TWO FINITE ELEMENT DISCRETIZATIONS
  - BASELINE (GRID POINT EVERY 8°)
  - REFINED (GRID POINT EVERY 2°)
- LOADING CONDITIONS
  - INTERNAL RADIAL PRESSURE ONLY
  - COMBINED INTERNAL PRESSURE AND AXIAL FORCE
  - PRE-LIFTOFF, TIME-CONSISTENT STS 51-L FLIGHT LOADS
- BOUNDARY CONDITIONS
  - BOTH ENDS SIMPLE-SUPPORT
  - ONE END SIMPLE-SUPPORT, OTHER END SYMMETRY

## SRB/ETA RING INTERFACE FINITE ELEMENT MODELS

The SRB/ETA ring interface models are developed using the original (i.e., STS 51-L) geometry configuration. Approximately sixty inches of the SRM motor case are modeled on either side of the SRB/ETA ring interface. Five shell units are used to model the SRM segments and stub rings. The ETA rings are modeled using an element unit and two user-written suboutines, USRPT and USRELT. User-written subroutine WALL is used to describe variations in the shell wall thickness as a function of longitudinal position. Listings of these FORTRAN subroutines are included in Appendices A, B, and C.

Two different finite element discretizations are considered. Both models have 26 elements along the length of the model. The baseline model has 45 elements uniformly-spaced circumferentially around the shell which corresponds to a node or grid point every eight degrees. The refined model has 180 elements uniformly-spaced circumferentially around the shell which corresponds to a node every two degrees. A listing of the STAGSC-1 input data for the baseline model is included in Appendix D.

Three loading conditions are considered. The first condition corresponds to internal pressure only; the second condition corresponds to internal pressure combined with an axial force. The axial force includes the axial component of the pressure load and the thrust load. For example, an internal pressure of 898.6 psi is combined with an axial force of 12.4 million pounds. The third condition corresponds to selected pre-liftoff, time-consistent loads for flight STS 51-L. Two sets of STS 51-L flight loads are considered; namely, those at maximum bending moment prior to SRM ignition (sometimes referred to as "max twang") and those just prior to liftoff but after the SRM ignition pressure transient. The applied loads for these conditions include SRM internal pressure, ET strut loads, and inplane shell loads.

The influence of boundary conditions on the overall shell response is also considered. One end of the finite element model (i.e., the aft end) corresponds to a factory joint in the SRM aft attachment segment and has been assumed to act as a simple-support boundary. At the other end of the model (i.e., the forward end), two conditions were investigated (symmetric and simple-support boundary conditions) since the SRB/ETA ring interface occurs within the overall SRB.

# MODELING ASSUMPTIONS

- TANG-CLEVIS JOINTS MODELED AS EQUIVALENT STIFFNESS JOINTS

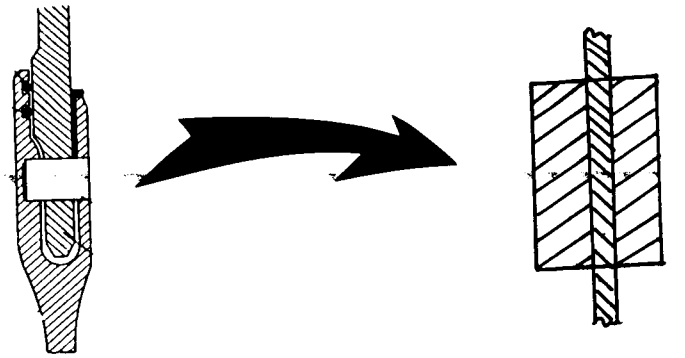

- "WELDED" CONNECTION BETWEEN ETA RING AND SRM STUB RING

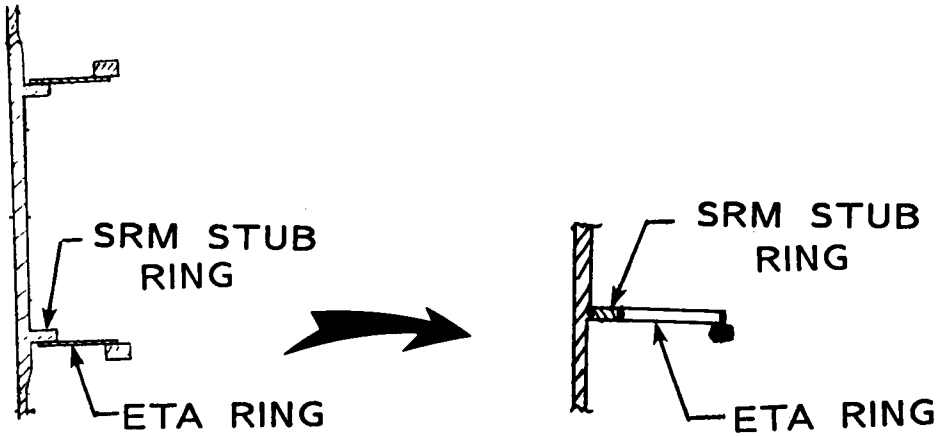


- NEGLECTED ETA RING COVER PLATES, INTERCOSTALS, AND H-FITTINGS

## MODELING ASSUMPTIONS

Two-dimensional shell finite element models of the portion of the SRB with the ETA ring have been developed using the STAGSC-1 computer code and executed on the NAS computers at the NASA Ames Research Center. The purpose of these analyses is to calculate the overall stress and deflection distributions for the SRB/ETA ring interface.

Both the field and the factory tang-clevis joints are modeled by using equivalent stiffness joints instead of detailed models of the joint. As such, the effect of local joints on the shell response is included; however, local joint behavior (i.e., gap motion) can not be obtained from these global models. Structural behavior of the local joints is described in reference 4. Global shell behavior of the SRB/ETA ring interface can be obtained using an equivalent stiffness joint, and an evaluation of nonlinear effects such as shell collapse and ovalization can be performed.

The properties for the equivalent stiffness joint are determined through parametric studies and comparisons with the referee test data[5]. These studies varied the SRM shell wall thickness in the vicinity of the joints. When a combination of thickness and effective length for the joints yields analytical results which agree with the measured radial deflections from the referee test girth gages, the equivalent stiffness joint properties are determined. In these analyses, the equivalent joint is modeled as a 6-inch-long portion of the shell with an 0.8-inch thickness.



The connection between the stub ring of the SRM aft attachment segment to the ETA rings is treated as a conventional finite element connection between adjacent elements in a model. This assumptions implies that the stub ring and the ETA ring are "welded" together or that these parts are "integrally machined". From the finite element analysis, equilibrium forces at the nodes or grid points are calculated. These equilibrium forces are related to the forces that must be carried by the bolted connection between the stub ring and the ETA ring.

The ETA ring web is modeled with one element through the depth of the web and has a uniform thickness of 0.25 inches. The ETA ring cap is modeled as a discrete stiffener with a rectangular cross section of 1.0 inches by 1.79 inches. The ETA ring cover plates, intercostals, H-fittings, and various other brackets are not included in these models.

# NONLINEAR SHELL ANALYSES

- BASELINE MODEL OF SRB/ETA RING INTERFACE
- REFINED MODEL OF SRB/ETA RING INTERFACE
- EFFECT OF BOUNDARY CONDITIONS
- EFFECT OF AXIAL LOAD
- EFFECT OF ET STRUT LOADS

## NONLINEAR SHELL ANALYSES

Nonlinear shell analyses for the baseline and refined discretizations of the SRB/ETA ring interface are presented in this paper. The effect of boundary conditions is described in relation to the shell response. The influence of the axial load on the overall shell response is also described. In addition, analytical results are presented for the nonlinear shell response corresponding to selected STS 51-L pre-liftoff loads.

# BASELINE MODEL OF SRB/ETA RING INTERFACE

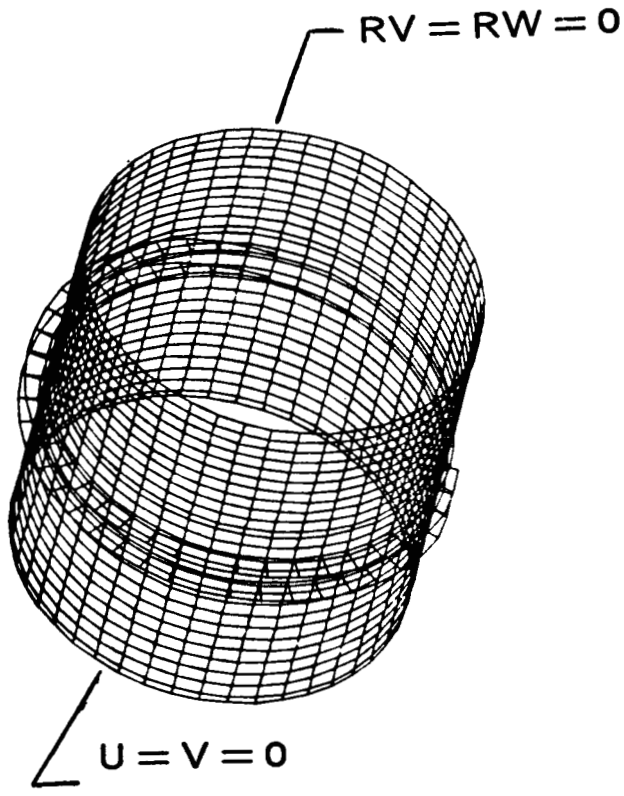


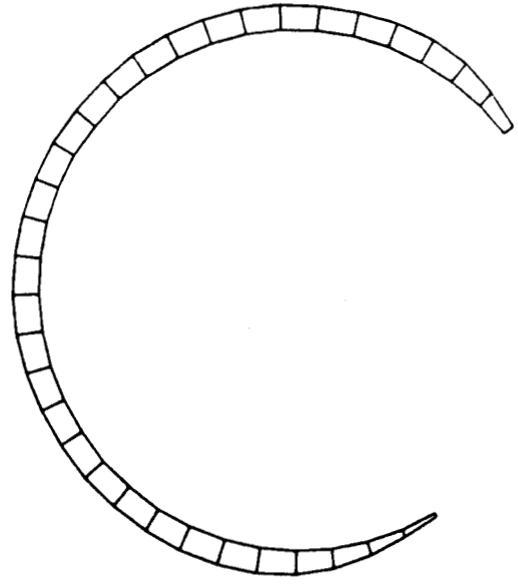

CROSS SECTION
OF
ETA RING
(8° per element)

- 411 element
- 46 by 26 Grid
- 11,905 d.o.f.
- Avg. semi-bandwidth of 510

## BASELINE MODEL OF SRB/ETA RING INTERFACE

The baseline finite element model of the SRB/ETA ring interface has 45 elements uniformly spaced around the shell circumference and 26 elements along its length. The finite element used in these analyses is designated as 411 in the STAGSC-1 element library. Symmetry boundary conditions are imposed at the forward end of the model with the exception that the longitudinal direction is unrestrained. Simple-support boundary conditions are imposed at the aft end of the model with the exception that the radial direction is unrestrained. This set of boundary conditions requires the aft end of the shell to remain circular.

Approximately 12,000 active degrees-of-freedom are in this finite element model. The average semi-bandwidth of the global stiffness matrix is 510. To form the elemental stiffness matrices and then assemble the global stiffness matrix required 19 CPU seconds on the NAS CRAY-2 computer. A single decomposition of the global stiffness matrix required an additional 100 CPU seconds. One forward-reduction/back-substitution cycle either to obtain the linear stress solution or to perform one nonlinear iteration required an additional 7 CPU seconds. The complete nonlinear shell analysis of the baseline model required a total of three decompositions of the global stiffness matrix and 16 nonlinear iterations.

# NONLINEAR SHELL RESPONSE

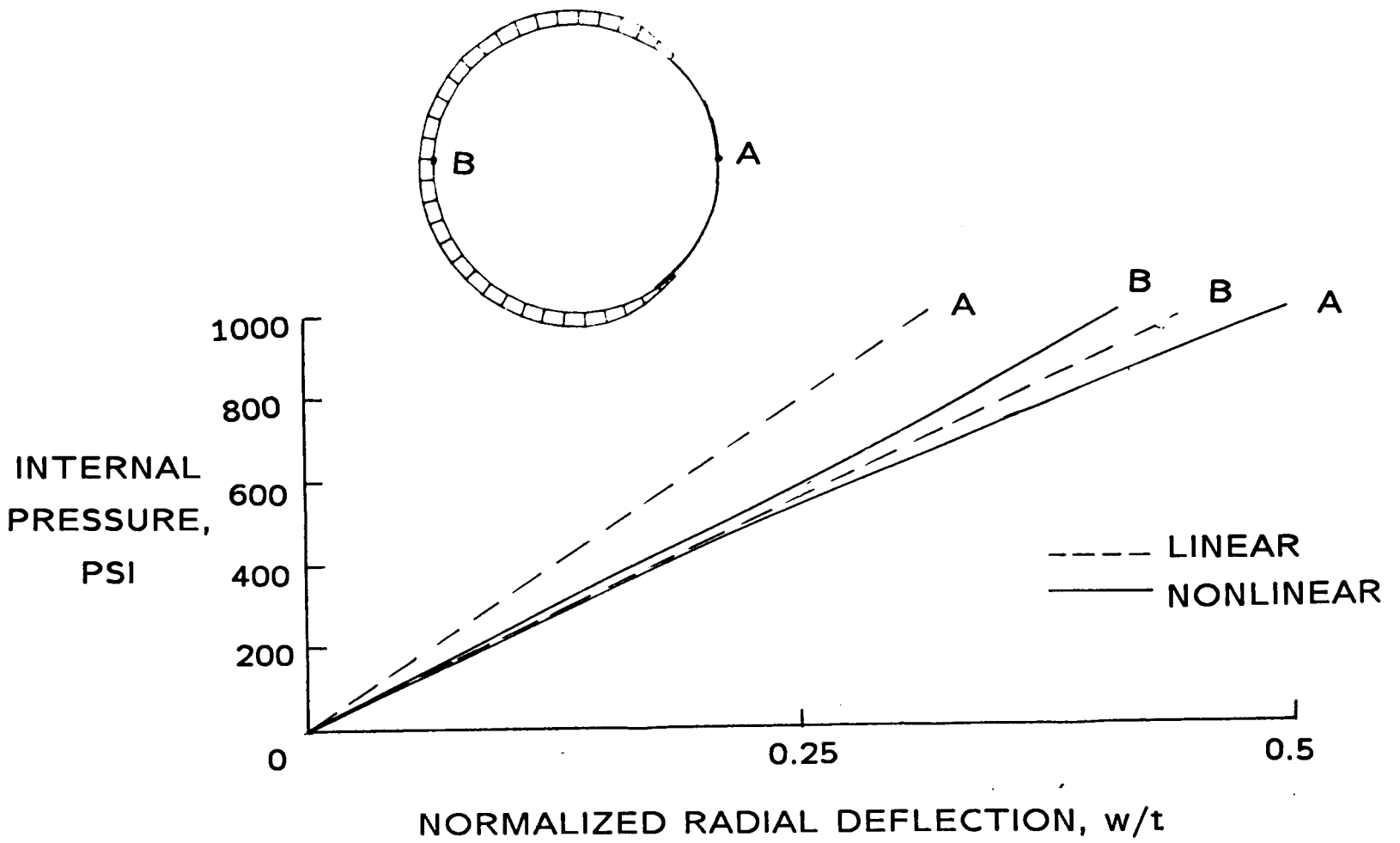

## NONLINEAR SHELL RESPONSE

The linear and nonlinear response of the radial deflection normalized by the nominal shell thickness (i.e., 0.479 inches) of two points diametrically opposite are shown in this figure as a function of internal pressure. The point labeled A is located midway between the ends of the ETA ring. The point labeled B is located approximately 180-degrees away and located on the ETA ring. The longitudinal location of these points is midway between the ETA ring webs (i.e., station 1511).

The shell response of point A exhibits significant nonlinearity. The radial deflection from the nonlinear solution for point A is nearly twice as large as the linear solution. Conversely, the shell response of point B is only mildly influenced by including the geometrically nonlinear effects and exhibits a stiffening trend.

# RADIAL DEFLECTIONS OF SRM STUB RING

(1000 psi INTERNAL PRESSURE ONLY)

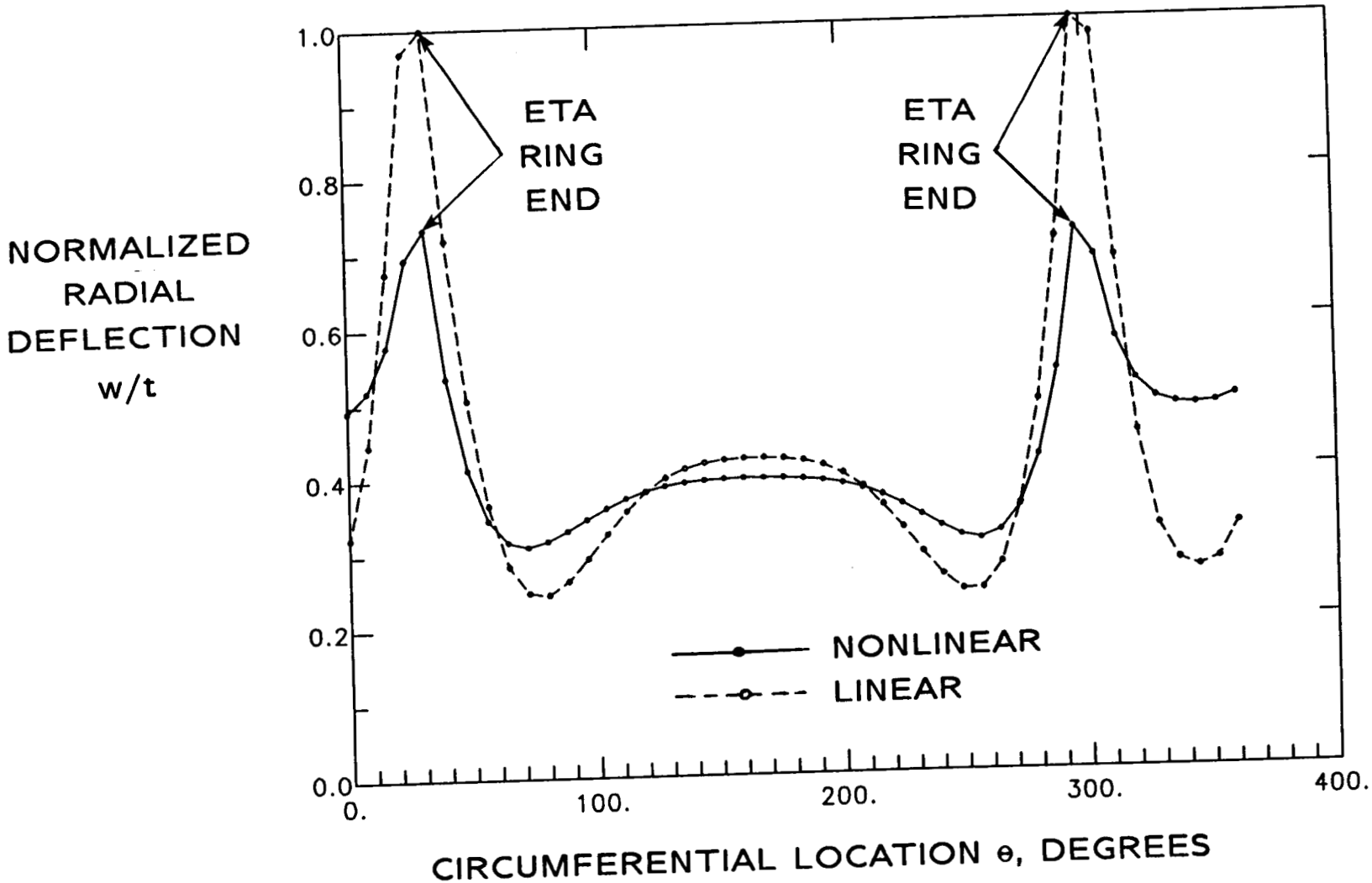

## RADIAL DEFLECTIONS OF SRM STUB RING

The radial deflection patterns of the SRM stub ring are shown in the figure for both the linear and nonlinear solutions. The radial deflections are normalized by the nominal shell thickness. At the ends of the ETA ring, the radial deflections from the linear analysis are equal to the shell thickness. This result indicates that a nonlinear analysis is required to predict accurately the structural response. The radial deflection pattern from the nonlinear analysis indicates a stiffening of the shell response due to the inclusion of geometric nonlinearities. These deflection patterns exhibit large changes in amplitude near the ends of the ETA ring.

# HOOP STRESS DISTRIBUTIONS OF SRM STUB RING

(1000 psi INTERNAL PRESSURE ONLY)

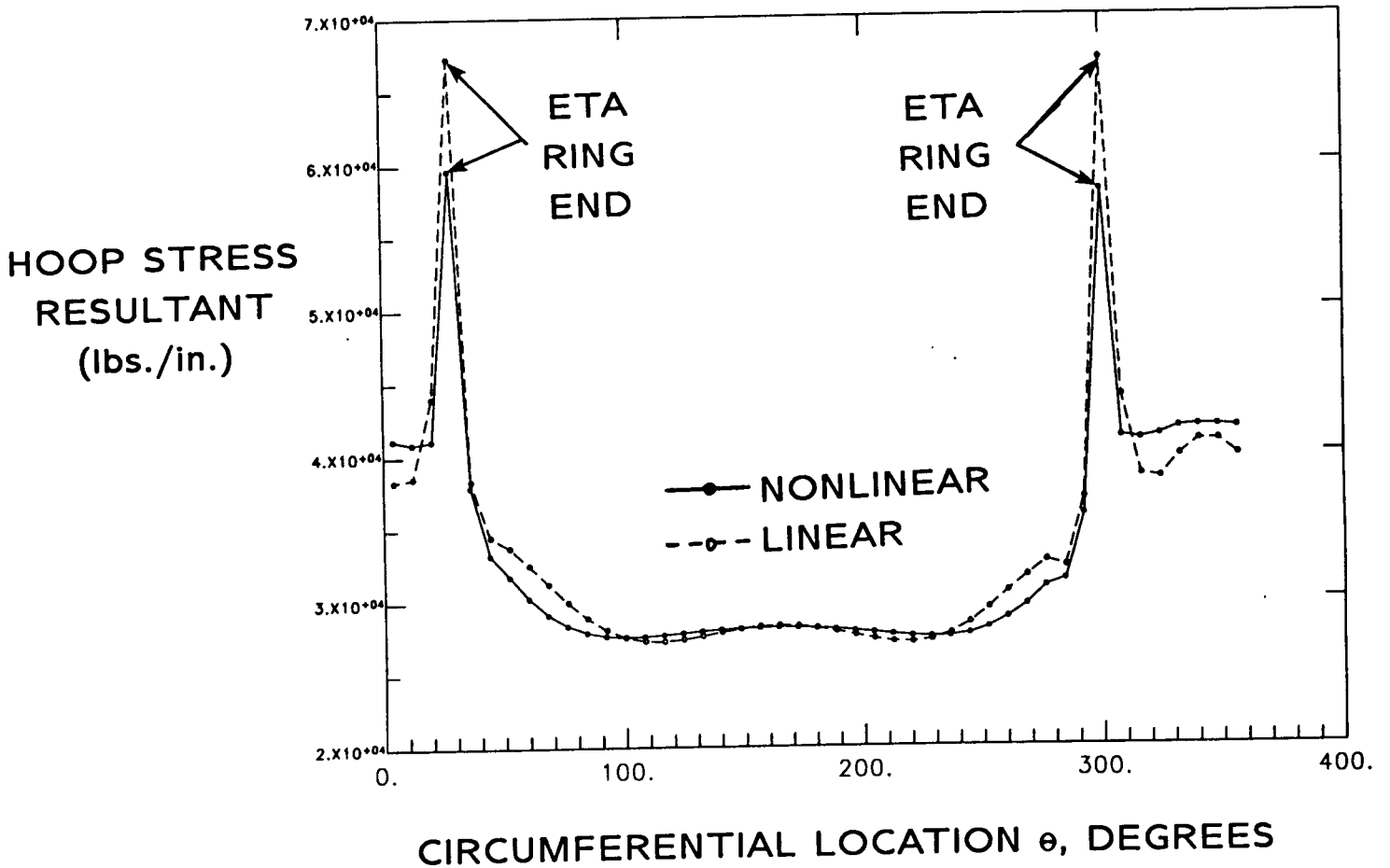

## HOOP STRESS DISTRIBUTIONS OF THE SRM STUB RING

The hoop stress distributions of the SRM stub ring are shown in the figure for the linear and nonlinear solutions. At the ends of the ETA ring, the hoop stress peaks due to the discontinuity in stiffness resulting from a partial ETA ring. The linear and nonlinear hoop stress distributions are similar, and their magnitudes are nearly the same except at the ends of the ETA ring. The nonlinear hoop stress at the end of the ETA ring is approximately 10% less than the linear hoop stress.

# DEFORMED GEOMETRIES OF BASELINE MODEL

(1000 psi INTERNAL PRESSURE ONLY)

LINEAR

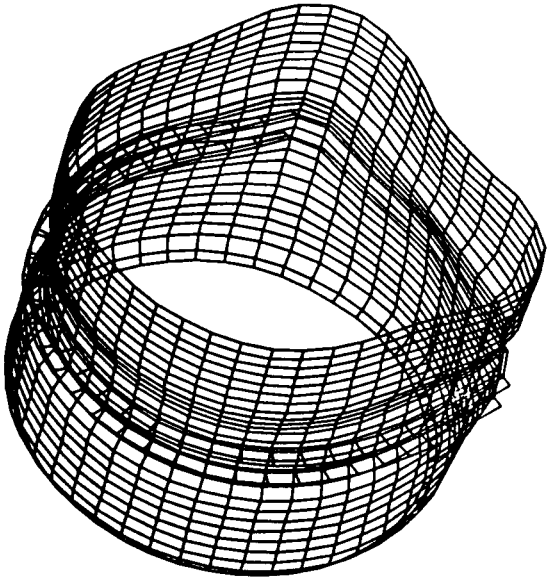

NONLINEAR

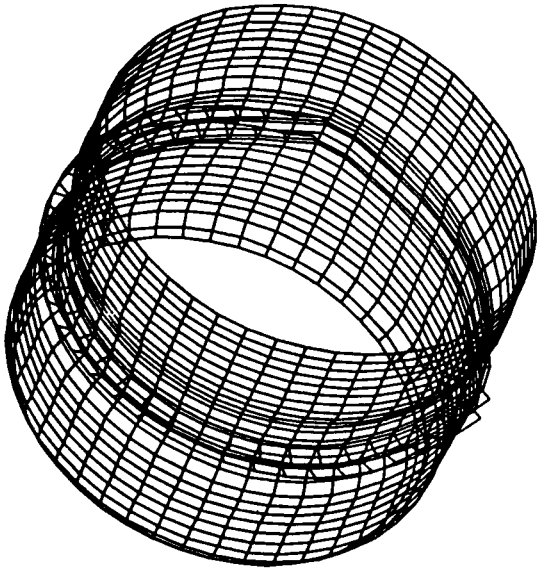

SRM STUB RING

LINEAR

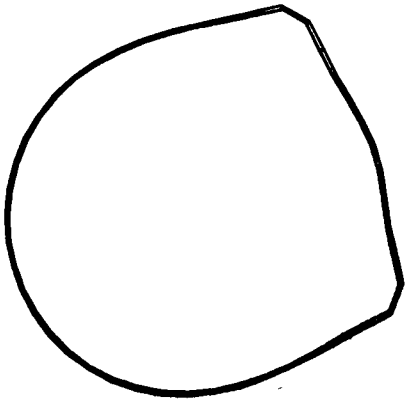

NONLINEAR

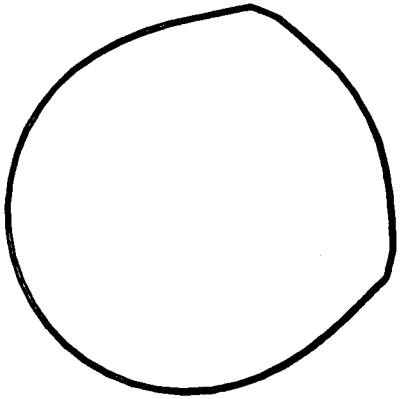

## DEFORMED GEOMETRIES OF BASELINE MODEL

The linear and nonlinear solutions for the baseline model of the SRB/ETA ring interface subjected to an internal pressure of 1000 psi are obtained. Deformed geometries with exaggerated deflections corresponding to the linear and nonlinear solutions are shown in the figure. Deformed geometries of the entire model are shown in the upper half of the figure and those of the SRM stub ring alone are shown in the lower half. Both the linear and nonlinear solutions exhibit an abrupt change in deflections near the ends of the ETA rings. This high local bending causes large tangential shearing and normal forces to develop between the SRM stub rings and the ETA rings.

# TANGENTIAL SHEARING FORCE DISTRIBUTION FOR BASELINE MODEL

(1000 psi INTERNAL PRESSURE ONLY)

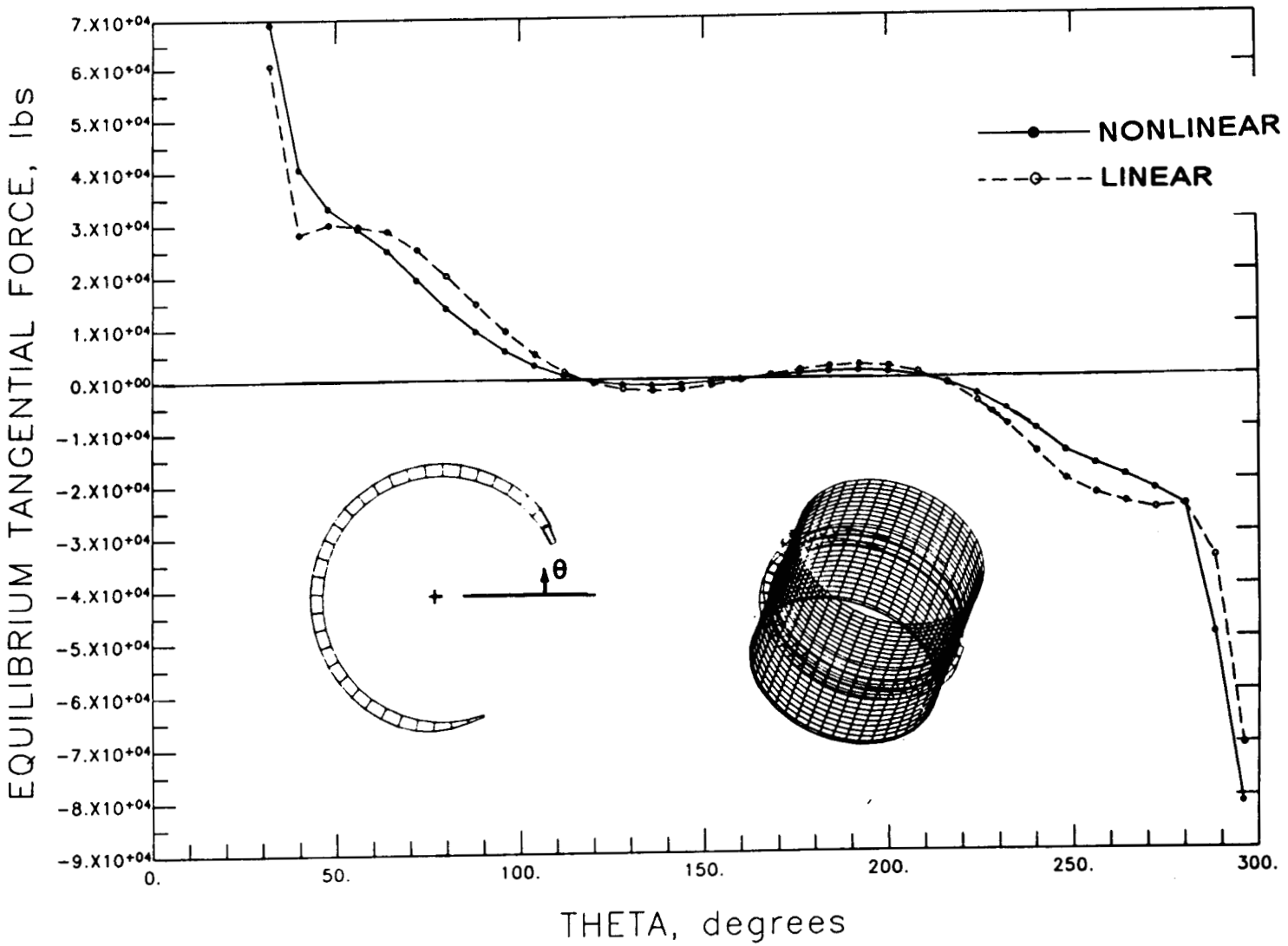

## TANGENTIAL SHEARING FORCE DISTRIBUTION FOR BASELINE MODEL

The tangential shearing force between the SRM stub ring and the ETA ring as a function of circumferential location is shown in the figure. The loading case considered is internal pressure only. Similar trends are shown for both the linear (dashed line) and nonlinear (solid line) solutions. Towards the middle of the ETA ring, the shearing force is small. As the ends of the ETA ring are approached, the shearing force increases; especially over the last few grid points. For the baseline model, the discretization is such that each grid point corresponds to approximately four bolted connections.

# AXIAL DISTRIBUTION OF NONLINEAR RADIAL DEFLECTIONS FOR BASELINE MODEL

(1000 psi INTERNAL PRESSURE ONLY)

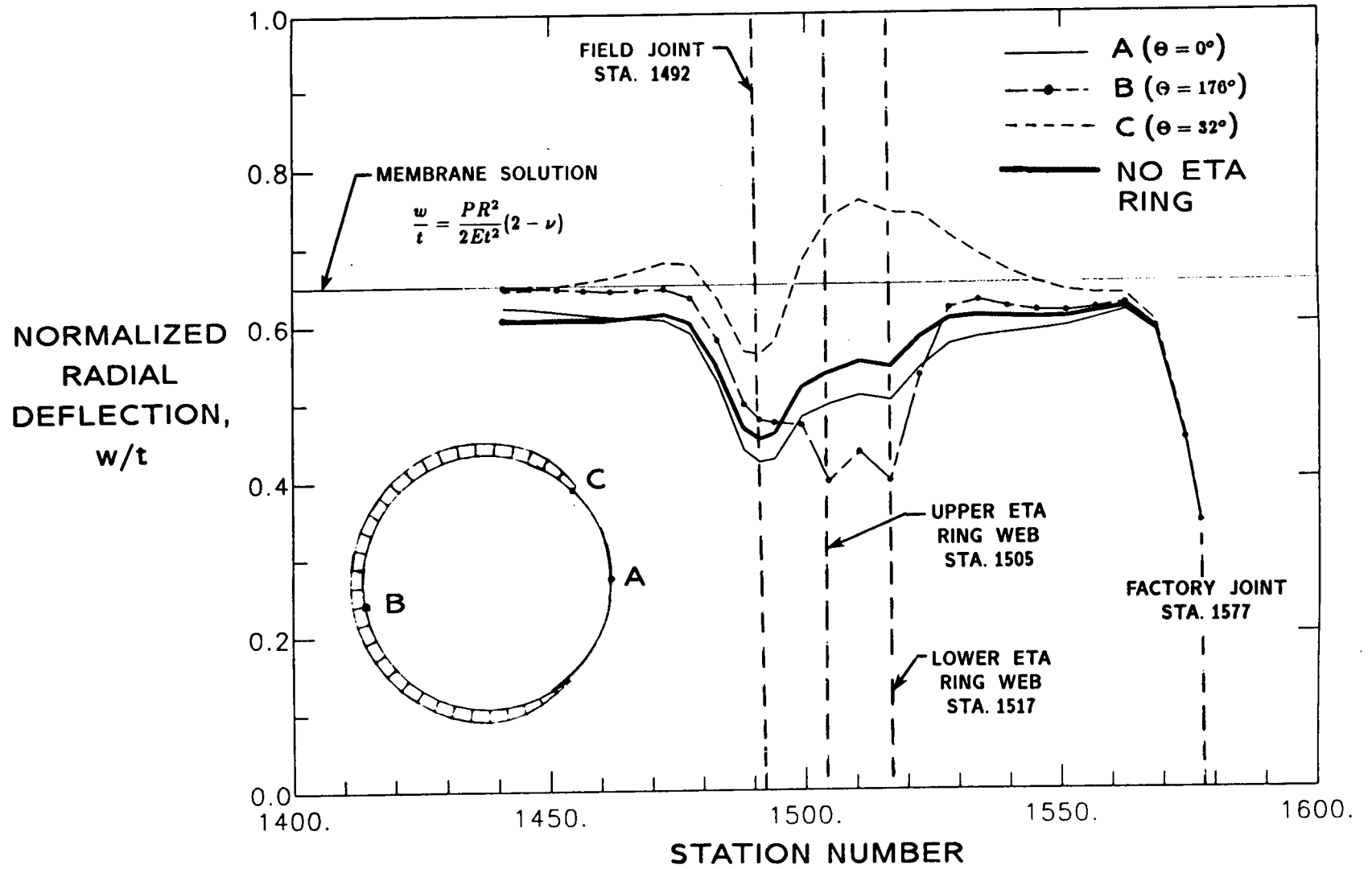

## AXIAL DISTRIBUTION OF NONLINEAR RADIAL DEFLECTIONS FOR BASELINE MODEL

The axial distribution of the nonlinear radial deflections for the baseline model subjected to 1000 psi internal pressure only is shown in the figure for three circumferential locations. The radial deflections are normalized by the nominal shell thickness and are shown as a function of SRB station number. Station numbers corresponding to tang-clevis joint (field and factory) locations and the upper and lower ETA ring webs are also noted on the figure.

The first circumferential location (point A) corresponds to midway between the ends of the ETA ring. The radial deflection pattern is denoted as the solid curve. This pattern exhibits a marked change in radial deflections near the field joint at station 1492 and is such that a tang-clevis joint would tend to open.

The second location corresponds to point B which is approximately 180 degrees opposite to point A. The radial deflection pattern at this location is denoted by a dashed line. The pattern near the field joint is again similar to the patterns at the other locations. However, near the ETA ring webs the radial deflection pattern is different and the stiffening influence of the ETA ring on the shell response can be seen.

The third location (point C) corresponds to an end of the ETA ring. The radial deflection at this location is denoted by a line with filled symbols. This pattern is similar to that of point A with the exception being an increase in amplitude of the radial deflections.



For comparison, two additional curves are shown on the figure. One curve represents the membrane solution, including the biaxial effect, for a uniform thickness (0.479 inches) cylindrical shell with an internal pressure of 1000 psi. The other curve represents the nonlinear solution for the same finite element model used to generate the other results except without the partial ETA ring.

These radial deflection patterns from the nonlinear solution also indicate that end effects due to imposed boundary conditions appear to be localized near the ends of the model. Also, these deflections patterns indicate that the STS 51-L tang-clevis field joint at station 1492 would tend to open. However, these models only reflect STS 51-L geometry and not the new SRM joint redesign with a capture feature. Extensive analytical studies are reported in reference 4 which describe the structural behavior of the original and modified tang-clevis joint designs. These studies included three-dimensional stress analysis, nonlinear contact, and correlation between test and analytical results.

# REFINED MODEL OF SRB/ETA RING INTERFACE

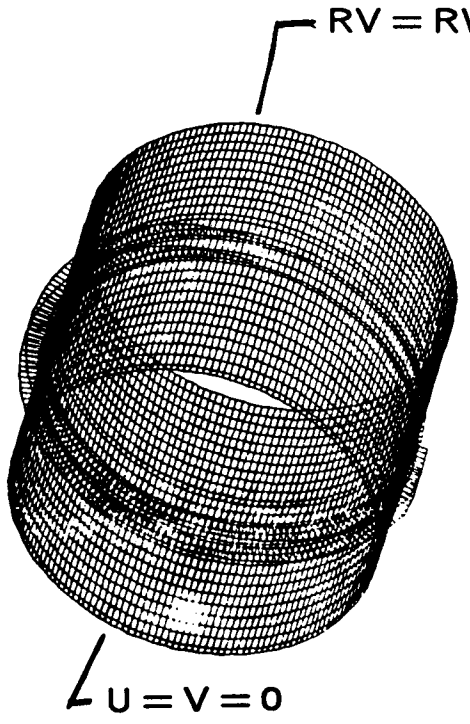


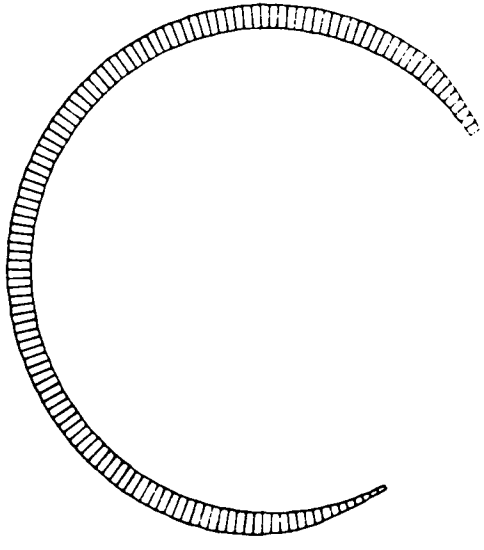

CROSS SECTION
OF
ETA RING
(2° per element)

- 411 element
- 181 by 26 Grid
- 47,572 d.o.f.
- Avg. semi-bandwidth of 512

## REFINED MODEL OF SRB/ETA RING INTERFACE

The refined model of the SRB/ETA ring interface has 180 elements uniformly spaced around the shell circumference and 26 elements along its length. The boundary conditions and loading for the refined model and the baseline model are identical. Results from the refined model are compared with those of the baseline model to assess the effects of circumferential discretization on the shell response. Only a linear elastic stress analysis is performed for this comparison.

Approximately 48,000 active degrees-of-freedom are in this finite element model. The average semi-bandwidth of the global stiffness matrix is 512. To form the elemental stiffness matrices and then assemble the global stiffness matrix required 57 CPU seconds on the NAS CRAY-2 computer. A single decomposition of the global stiffness matrix required an additional 410 CPU seconds. One forward-reduction/back-substitution cycle either to obtain the linear stress solution or to perform one nonlinear iteration required an additional 15 CPU seconds.

# DEFORMED GEOMETRIES OF REFINED MODEL

(1000 psi INTERNAL PRESSURE ONLY)

LINEAR ANALYSIS

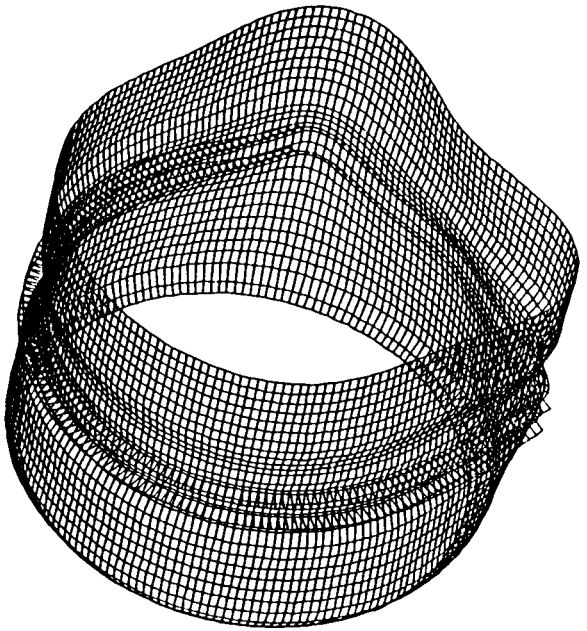

SRM STUB RING

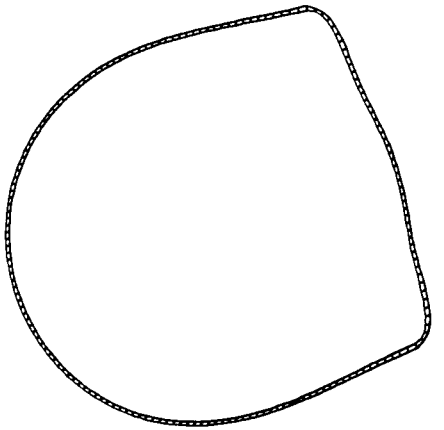

## DEFORMED GEOMETRIES OF REFINED MODEL

The linear solution for the baseline model of the SRB/ETA ring interface subjected to an internal pressure of 1000 psi is obtained for comparison with the linear solution for the baseline model. Deformed geometries with exaggerated deflections corresponding to the linear solution are shown in the figure. The deformed geometry of the entire model is shown on the left of the figure and that of the SRM stub ring alone is shown in the right. The linear solutions from both the baseline and refined models exhibit the same abrupt change in deflections near the ends of the ETA rings. However, a smoother transition is shown for the refined model.

# TANGENTIAL SHEARING FORCE DISTRIBUTION FOR REFINED MODEL

(1000 psi INTERNAL PRESSURE ONLY)

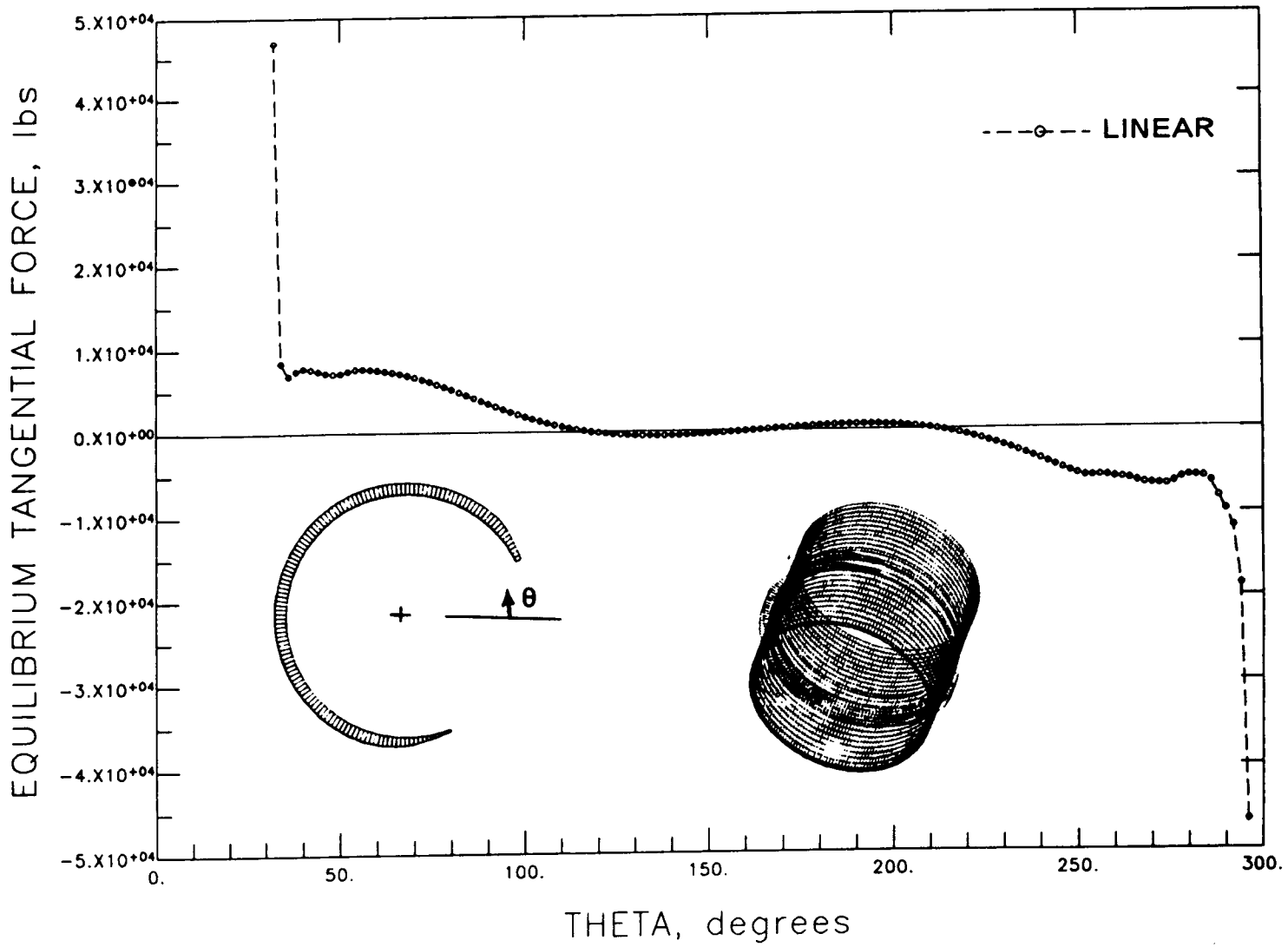

## TANGENTIAL SHEARING FORCE DISTRIBUTION FOR REFINED MODEL

The tangential shearing force between the SRM stub ring and the ETA ring as a function of circumferential location is shown in the figure. The loading case considered is internal pressure only. Similar trends are shown for both the refined and baseline models. Towards the middle of the ETA ring, the shearing force is small. As the ends of the ETA ring are approached, the shearing force increases; especially over the last several grid points. For the refined model, the discretization is such that each grid point corresponds to approximately one bolted connection. The main effect of increased discretization in the circumferential direction is the better approximation of the deformed shapes and force distributions in that direction. The overall shell behavior remained the same for the two discretizations considered, and as such, the baseline model is used for the remaining analyses presented in this paper.

# SHELL RESPONSE
# FOR SIMPLE SUPPORT BOUNDARY CONDITIONS

LINEAR

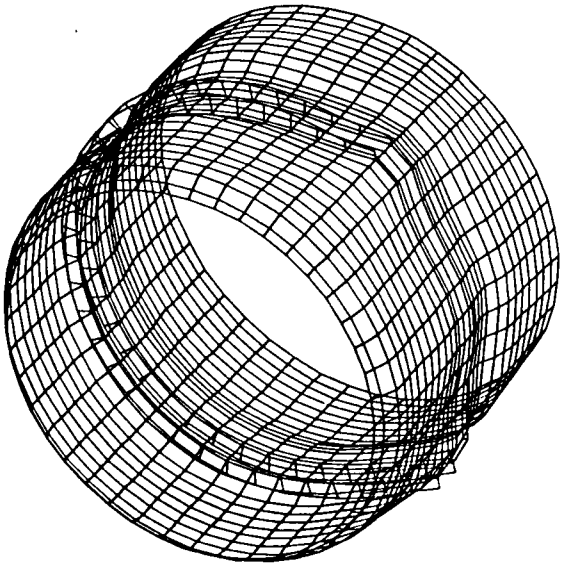

NONLINEAR

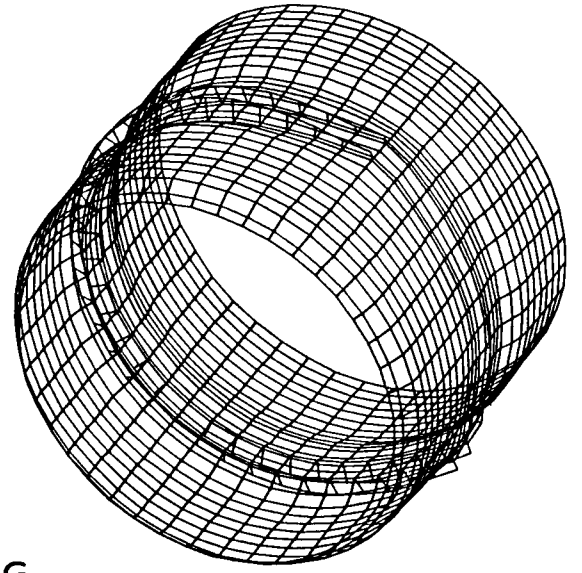

SRM STUB RING

LINEAR

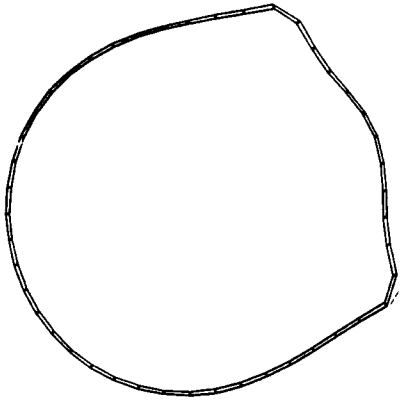

NONLINEAR

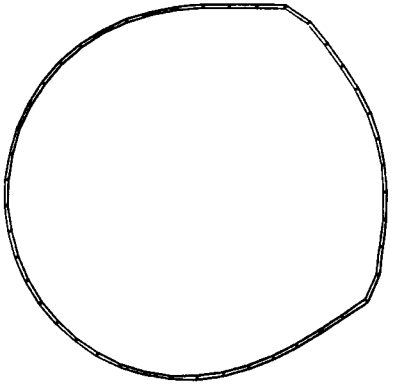

## SHELL RESPONSE FOR SIMPLE SUPPORT BOUNDARY CONDITIONS

For the baseline model, symmetry boundary conditions are imposed at the forward end of the model and simple-support conditions are imposed at the aft end. This set of boundary conditions requires the aft end of the shell to remain circular. The aft end corresponds to a "factory joint" in the SRM. The effect of boundary conditions on the shell response is assessed by changing the boundary conditions at the forward end from symmetric to simple-support conditions.

The linear and nonlinear solutions of the SRB/ETA ring interface subjected to an internal pressure of 1000 psi are obtained for this additional set of boundary conditions. Deformed geometries with exaggerated deflections corresponding to the linear and nonlinear solutions are shown in the figure. Again, both the linear and nonlinear solutions exhibit an abrupt change in deflections near the ends of the ETA rings. This high local bending causes large tangential shearing and normal forces to develop between the SRM stub rings and the ETA rings.

The effect of boundary conditions on the shell response is more dramatic for the linear solutions than for the nonlinear solutions. Changing the boundary conditions from symmetric to simple-support caused the forward end to remain circular. As such, the deformed shape in the longitudinal direction changed from a long wavelength pattern to a shorter wavelength pattern. With symmetric boundary conditions at the forward end, the deflection pattern of the linear solution is characterized by a flattening of the SRM stub ring in the region without the ETA ring. Comparison of the deformed geometries for the nonlinear solutions do not reveal any marked change resulting from a change in boundary conditions at the forward end of the model.

# EFFECT OF BOUNDARY CONDITIONS ON SHELL RESPONSE

(1000 psi INTERNAL PRESSURE ONLY)

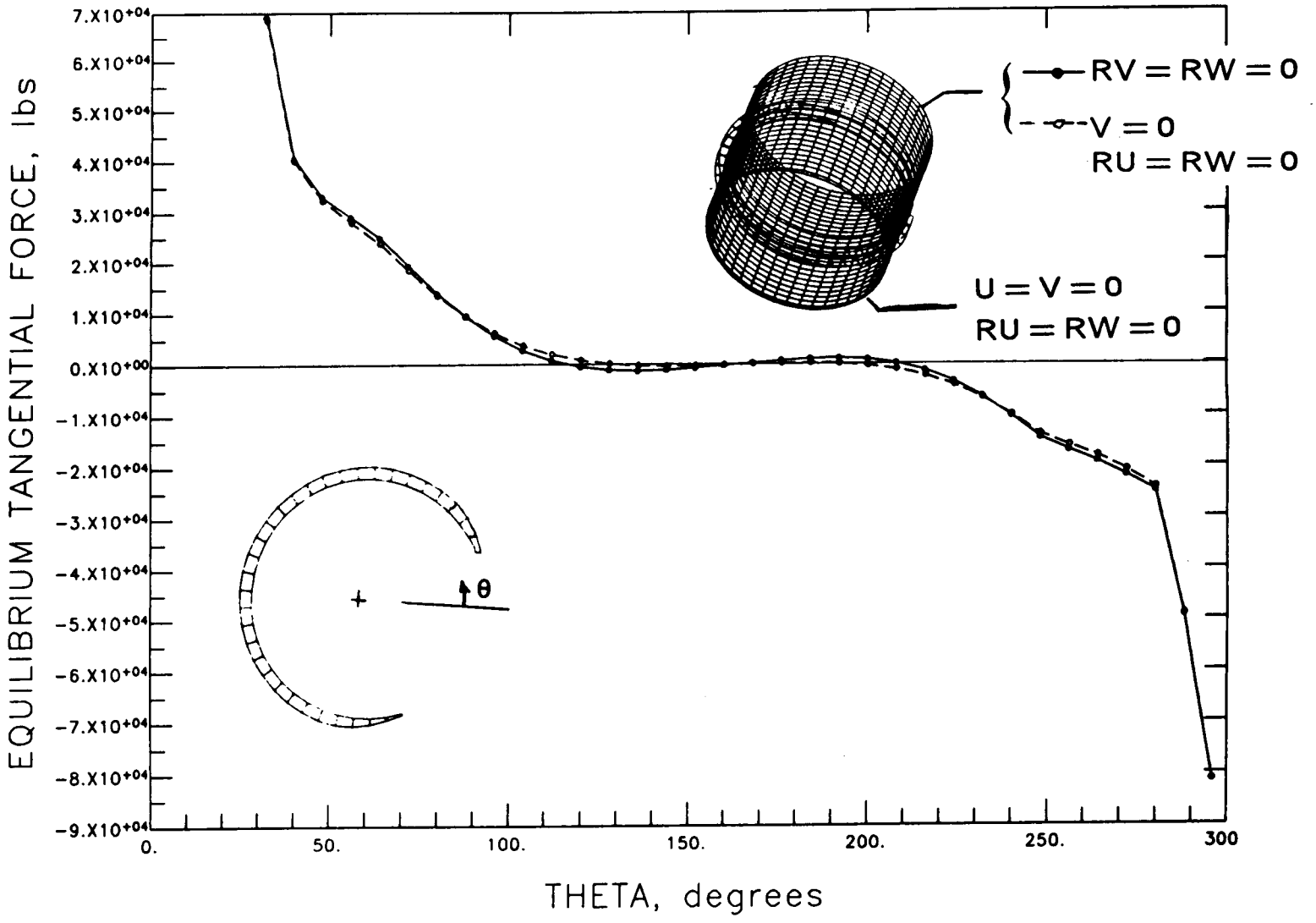

## EFFECT OF BOUNDARY CONDITIONS ON SHELL RESPONSE

The tangential shearing force between the SRM stub ring and the ETA ring as a function of circumferential location is shown in the figure for two sets of boundary conditions applied at the forward end. The loading case considered is internal pressure only. Comparison of the tangential shearing force distribution for the symmetric (solid line) and simple-support (dashed line) boundary conditions is shown in the figure for the nonlinear solutions. Similar trends are shown for both sets of boundary conditions. Towards the middle of the ETA ring, the shearing force is small. As the ends of the ETA ring are approached, the shearing force increases; especially over the last few grid points. For the baseline model, the discretization is such that each grid point corresponds to approximately four bolted connections. These results indicate that tangential shearing force distributions are not influenced by these two sets of boundary conditions.

# EFFECT OF COMBINED LOAD ON SHELL RESPONSE

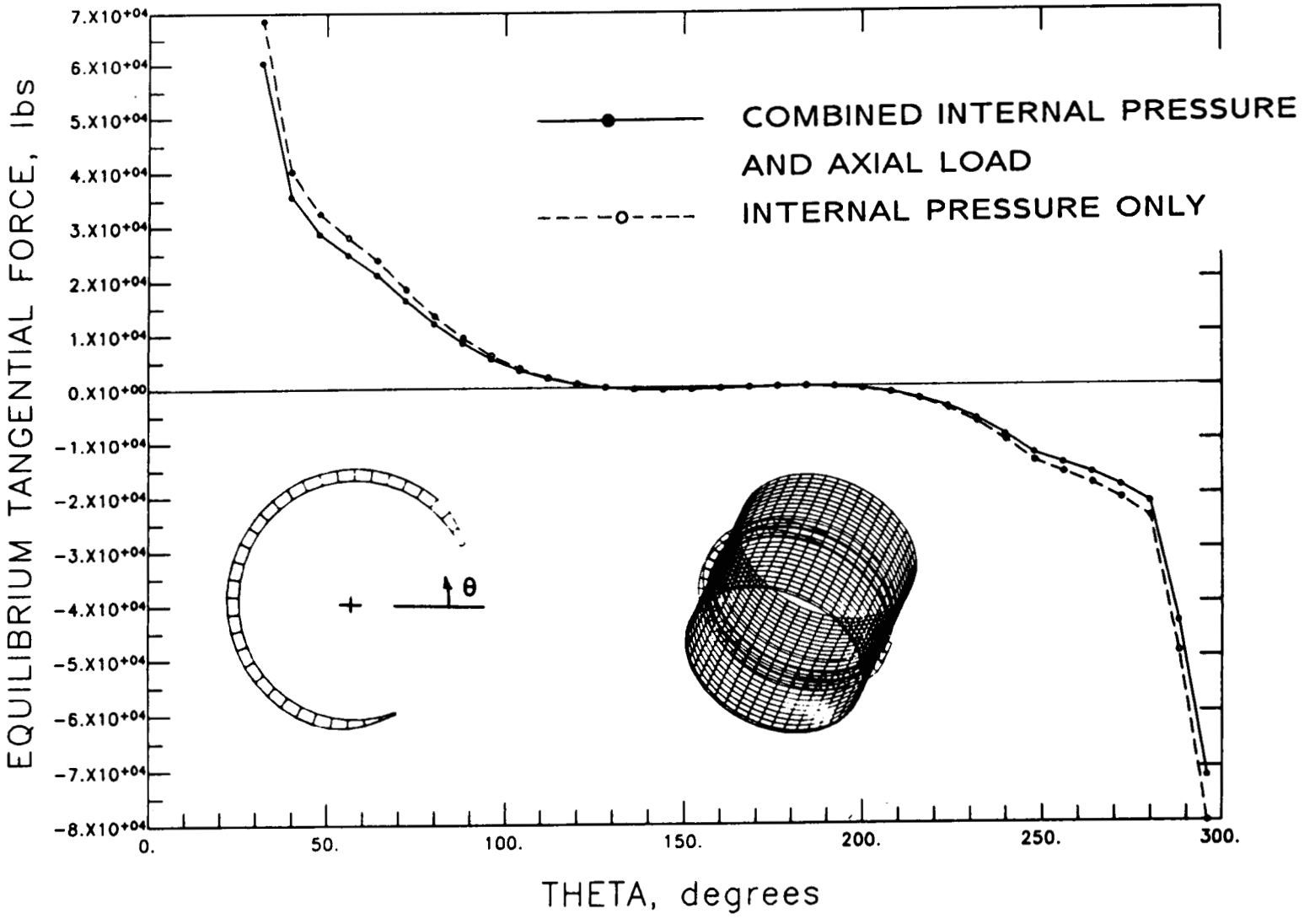

## EFFECT OF COMBINED LOAD ON SHELL RESPONSE

The tangential shearing force between the SRM stub ring and the ETA ring as a function of circumferential location is shown in the figure for two loading conditions. The boundary conditions at the aft end are symmetry and those at the forward end are simple-support. Comparison of the tangential shearing force distributions for the pressure only case (dashed line) and the combined pressure and axial force case (solid line) is shown in the figure for the nonlinear solutions. Similar trends are shown for both loading cases. The shell response is not sensitive to the axial load. Since the axial load is tensile, the combined load case represents a slightly stiffer structural response.

# OVERVIEW OF PRE-LIFTOFF LOADS TRANSIENT

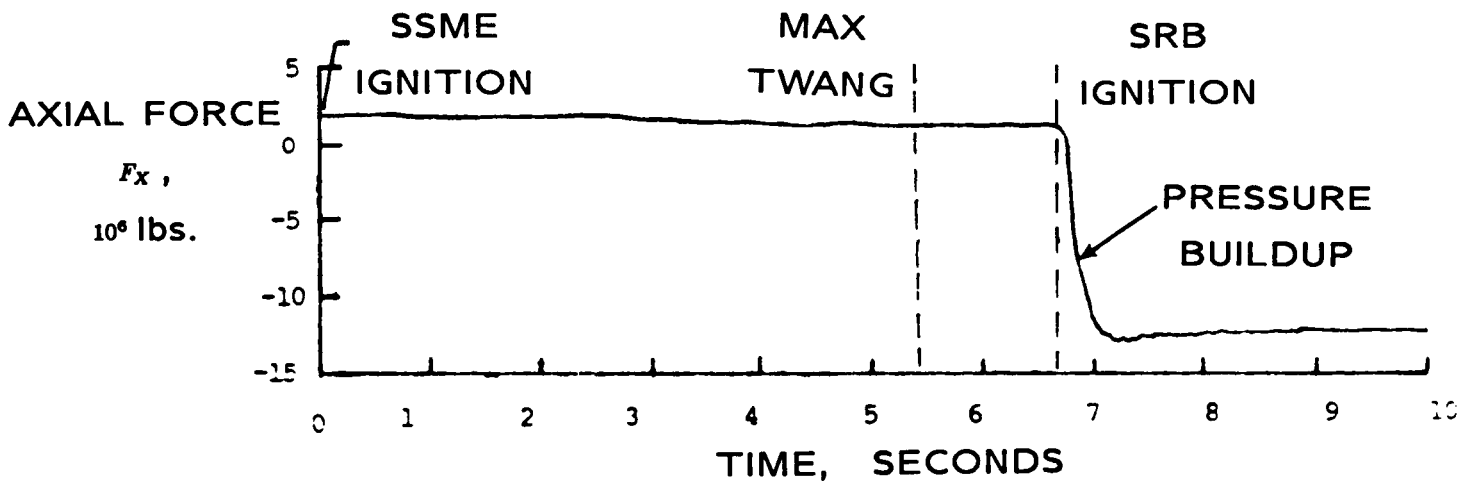


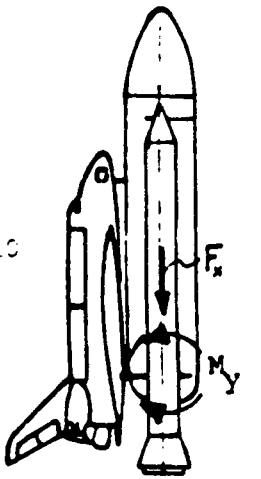


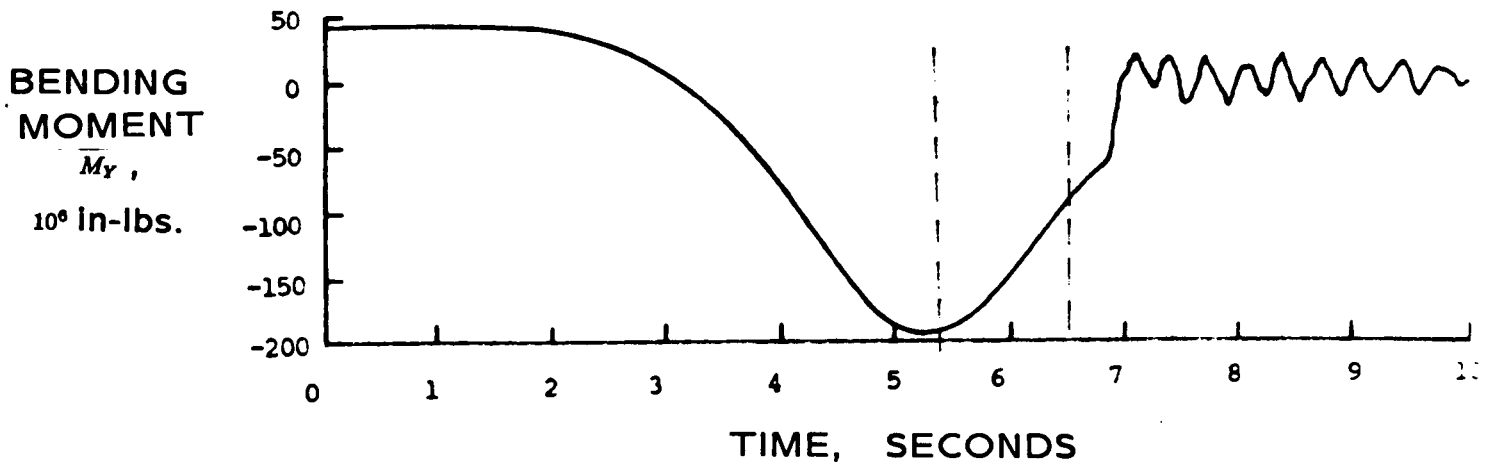

## OVERVIEW OF PRE-LIFTOFF LOADS TRANSIENT

An overview of the pre-liftoff loads variations after SSME ignition is briefly described. At t = 0, the loads induced into the SRB are due to the eccentric weight of the orbiter and the external fuel tank and due to cryogenic shrinkage of the external tank during tanking. At SSME ignition, an eccentric thrust of approximately one million pounds is produced that causes the space shuttle to bend over to a maximum deflection (referred to as max twang) and then spring back towards its original static configuration. For STS 51-l, the maximum bending occurred at t = 5.3 seconds. The SSME reached full thrust approximately 6.6 seconds after ignition. At t = 6.6 seconds, the space shuttle system has fully rebounded and the signal is issued to ignite the solid rocket motor propellant. The SRM ignition pressure transient has a duration of approximately 600 milliseconds for the pressure to build up inside the solid rocket boosters.

# SELECTED STS 51-L PRE-LIFTOFF LOADING CASES

| | Time After SSME Ignition, seconds | |
|---|---|---|
| | t = 5.3 | t = 7.2 |
| Equivalent Beam Loads | | |
| $F_x$, lb. | 1,252,029 | -12,906,980 |
| $F_y$, lb. | 61,859 | 109,565 |
| $F_z$, lb. | -200,345 | 1,185 |
| $M_x$, in.-lb. | 13,879,510 | 313,331 |
| $M_y$, in.-lb. | -194,578,500 | -2,544,368 |
| $M_z$, in.-lb. | -28,056,290 | -4,455,716 |
| Et Strut Loads | | |
| P8, lb. | 41,188 | 109,626 |
| P9, lb. | 93,003 | 65,442 |
| P10, lb. | -10,042 | -22,958 |
| SRM Internal Pressure | | |
| P, psi | 0 | 1000 |

## SELECTED STS 51-L PRE-LIFTOFF LOADING CASES

The reconstructed flight loads for the STS 51-L right SRB were obtained from NASA Johnson Space Center (JSC) initially in the form of strip charts and later in the form of data stored on a magnetic tape. The loads data consist of equivalent beam forces and moments, and vehicle interface loads for the first ten seconds of the flight. The equivalent beam forces and moments are given at 19 locations along the right SRB and include inertial effects. The interface loads are components of the loads in the forward and aft struts connecting the right SRB to the ET. The loading cases considered in these analyses correspond to the time-consistent loads at t = 5.3 and 7.2 seconds after SSME ignition.

The reconstructed beam forces and moments for the SRB/ETA ring interface shell analysis model including the aft ET strut loads are shown in the figure. The aft ET attachment loads are equally divided between the two ETA ring webs and applied as point forces. The reconstructed beam loads are converted to shell loads and applied as point forces distributed around the shell circumference.

# EQUIVALENT SHELL LOADS

RECONSTRUCTED BEAM FORCES AND MOMENTS REPLACED BY STATICALLY EQUIVALENT SET OF $N_x$ AND $N_{x\theta}$ STRESS RESULTANTS

$$N_x = \frac{-F_x}{(2\pi R)} + \frac{[M_z\ sin\theta - M_y\ cos\theta]}{(\pi R^2)}$$

$$N_{x\theta} = \frac{-M_x}{(2\pi R^2)} + \frac{[F_z\ sin\theta - F_y\ cos\theta]}{(\pi R)}$$

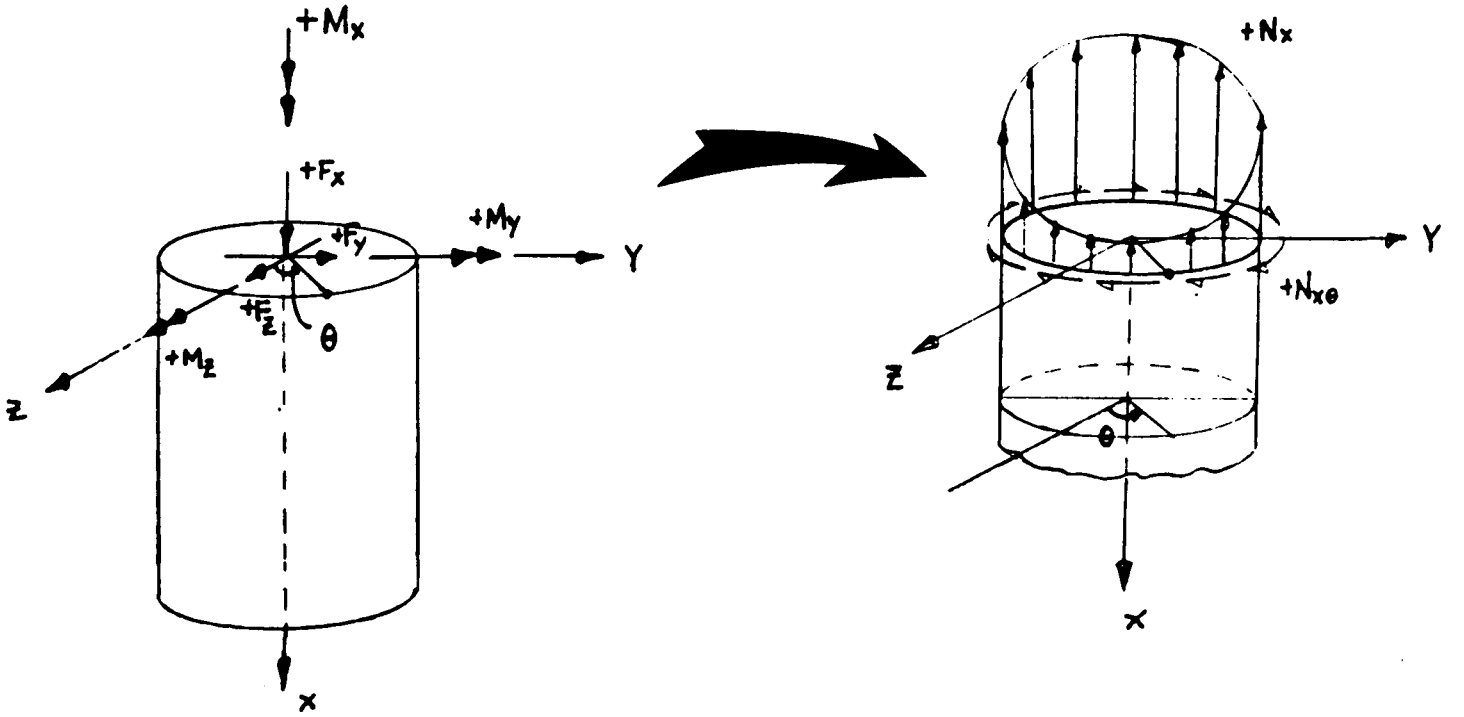

## EQUIVALENT SHELL LOADS

Using the flight loads from JSC, the reconstructed beam forces and moments are used to generate a statically equivalent set of shell stress resultants for inplane compression and shear. The relationship between the beam forces and moments and the equivalent shell resultants is given on the figure. The shell resultants have a circumferential distribution similar to that shown on the lower right of the figure.

# NONLINEAR RADIAL DEFLECTIONS OF SRM STUB RING SUBJECTED TO SELECTED STS 51-L PRE-LIFTOFF LOADS

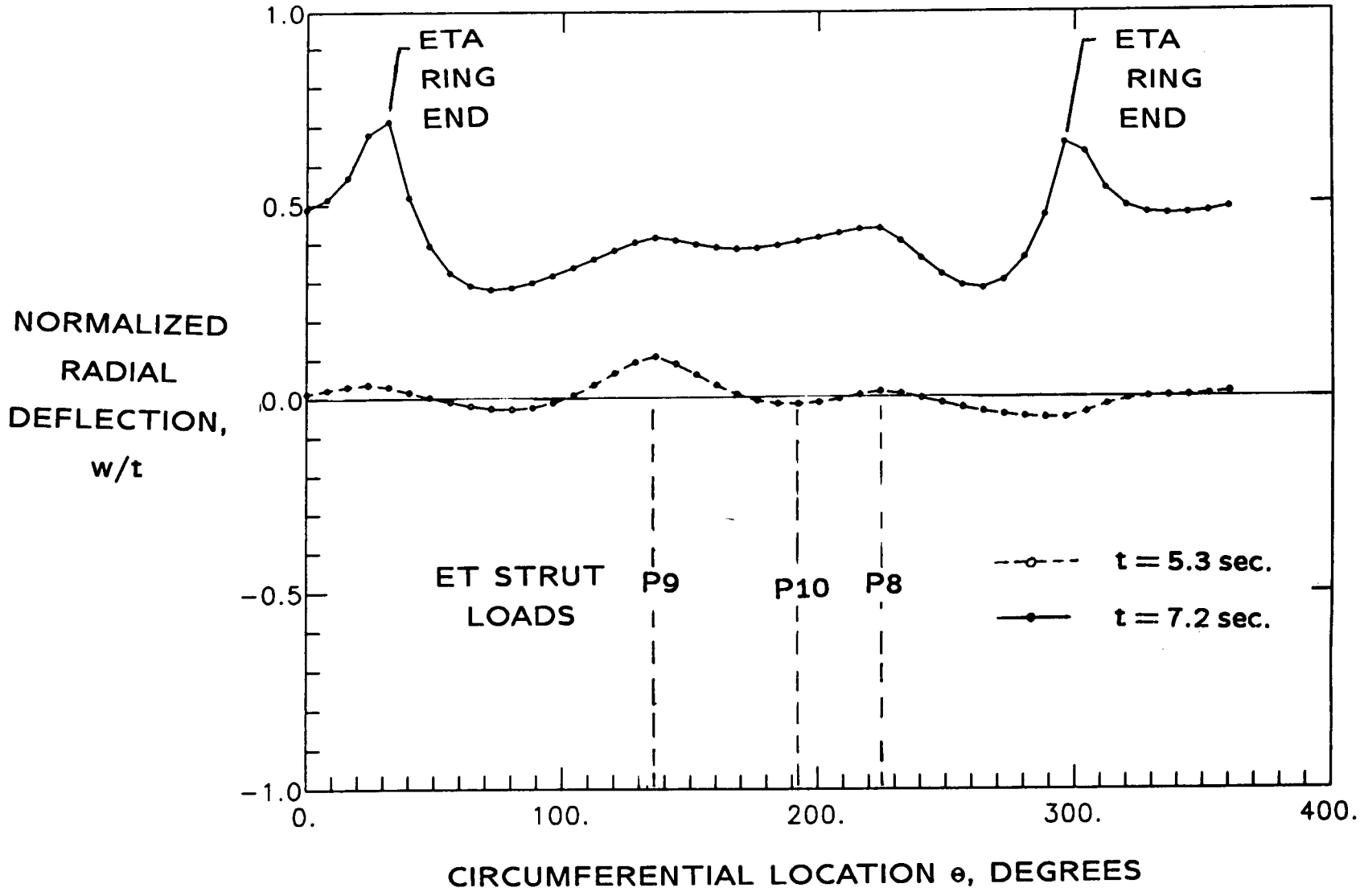

## NONLINEAR RADIAL DEFLECTIONS OF SRM STUB RING SUBJECTED TO SELECTED STS 51-L PRE-LIFTOFF LOADS

Nonlinear analyses of the SRB/ETA ring interface model using the reconstructed loads for time t=5.3 and 7.2 seconds after SSME ignition have been performed. Time t=5.3 seconds corresponds to the time at which maximum bending occurs and has been referred to as "max twang". At this time, the SRM is unpressurized since it has not yet been ignited. Time t=7.2 seconds corresponds to the time at which the SRM reaches full pressure and liftoff occurs. These analyses included the asymmetric loads resulting from the aft ET strut loads and the equivalent shell loads.

Two STS 51-L pre-liftoff, time-consistent loading cases have been considered. The ET strut loads at maximum bending result in an asymmetric radial deflection pattern; however, the amplitudes of these deflections are small compared to either the nominal shell thickness or the radial deflections caused by internal pressure loading only.

# NONLINEAR SHELL RESPONSE
# FOR SELECTED STS 51-L PRE-LIFTOFF LOADS

MAX. TWANG

(t = 5.3 sec.)

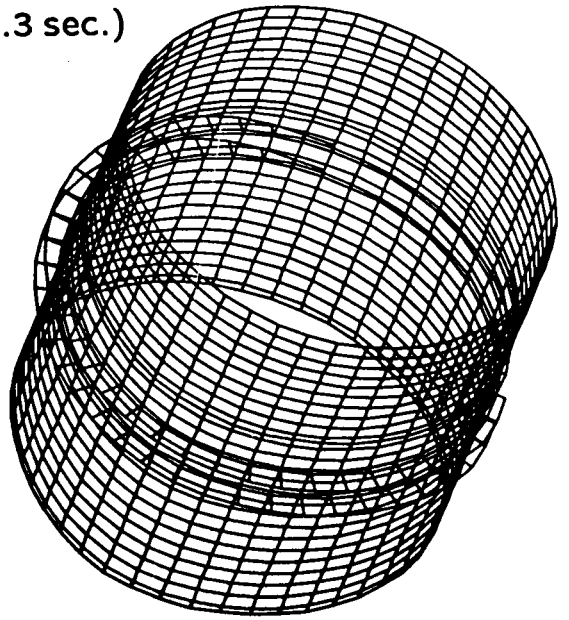

SRM PRESSURIZATION

(t = 7.2 sec.)

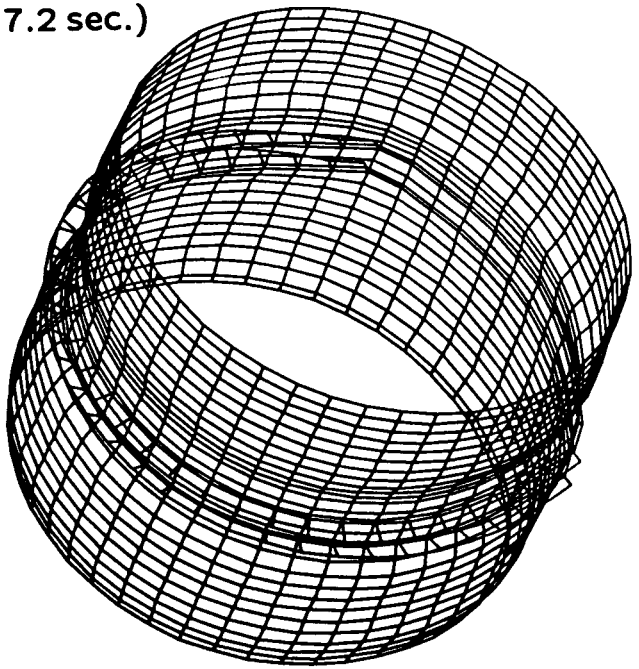

SRM STUB RING

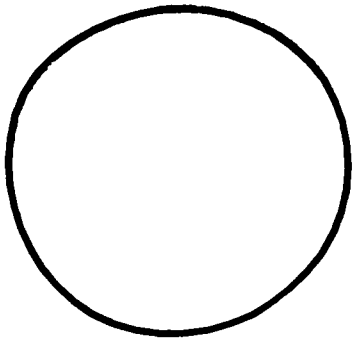

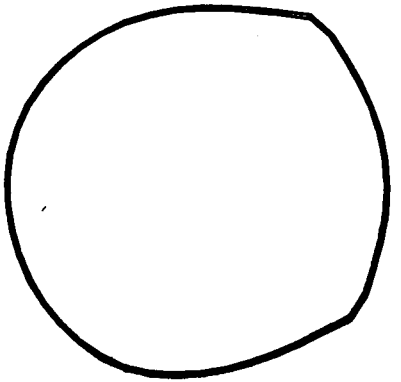

## NONLINEAR SHELL RESPONSE FOR SELECTED STS 51-L PRE-LIFTOFF LOADS

The nonlinear solutions for the baseline model of the SRB/ETA ring interface subjected to STS 51-L pre-liftoff loads at t=5.3 and 7.2 seconds after SSME ignition are obtained. Deformed geometries of the entire model are shown in the upper half of the figure and those of the SRM stub ring alone are shown in the lower half. The deformed geometries shown on the left correspond to the loading case at t=5.3 seconds. Even though the deflections have been exaggerated, only a slight amount of deflection is noticeable. The deformed geometries shown on the right correspond to the loading case at t=7.2 seconds which includes SRM pressurization. At SRM pressurization, the overall shell response is dominated by the effects of the internal pressure, and the effect of the ET strut loads is secondary.

# SUMMARY

- LINEAR AND NONLINEAR DEFLECTION PATTERNS SIGNIFICANTLY DIFFERENT
- LINEAR AND NONLINEAR TANGENTIAL SHEARING FORCE DISTRIBUTIONS SLIGHTLY DIFFERENT
- LINEAR SHELL RESPONSE SENSITIVE TO BOUNDARY CONDITIONS; NONLINEAR SHELL RESPONSE NEARLY INSENSITIVE
- AXIAL FORCE STIFFENS SHELL, REDUCES RADIAL DEFLECTIONS; ONLY SLIGHT INFLUENCE ON SHELL RESPONSE
- ET STRUT LOADS ARE SECONDARY COMPARED TO SRM PRESSURE

## SUMMARY

Overviews of the SRB/ETA ring interface geometry and finite element models used for the nonlinear shell analyses have been presented in this paper. The overall stress and deflection distributions for the SRB/ETA ring interface have been presented. These analytical results indicate significant differences between the linear and nonlinear deflections patterns for the SRB/ETA ring interface. However, only a slight difference has been shown between the linear and nonlinear tangential shearing force distributions. The linear shell response has been shown to be sensitive to boundary conditions while the nonlinear solutions appear to be nearly insensitive.

The loading component which has been shown to significantly affect the shell deflection patterns is the SRM internal pressure. Both the deflection pattern and the tangential shearing force distribution changed only slightly when an axial force was combined with the internal pressure loading case. Two STS 51-L pre-liftoff, time-consistent loading cases have been considered. The ET strut loads at maximum bending result in an asymmetric radial deflection pattern; however, the amplitudes of these deflections are small compared to either the nominal shell thickness or the radial deflections caused by internal pressure loading only. At SRM pressurization, the overall shell response has been shown to be dominated by the effects of the internal pressure.

## REFERENCES


1. *Report of the Presidential Commission on the Space Shuttle Challenger Accident*, Washington, D.C., June 6, 1986.

2. Almroth, B. O.; Brogan, F. A.; and Stanley, G. M.: *Structural Analysis of General Shells, Vol. II, User Instructions for STAGSC-1*, Report No. LMSC-D633873, Lockheed Palo Alto Research Laboratory, Palo Alto, CA, December 1982.

3. Rankin, C. C.; Stehlin, P.; and Brogan, F. A.: *Enhancements to the STAGS Computer Code*, NASA CR-4000, November 1986.

4. Greene, William H.; Knight, Norman F., Jr.; and Stockwell, Alan E.: *Structural Behavior of the Space Shuttle SRM Tang-Clevis Joint*, NASA TM-89018, September 1986.

5. Oostyen, J. E.; Bright, D. D.; Hawkins, G. F.; McCluskey, P. M.; and Larsen, G. L.: *SRM Joint Deflection Referee Test: Phase 2 Final Report*, Morton Thiokol, Inc., Wasatch Operations, Document Number TWR-300149, April 3,1986.

# Appendix A: User-Written Subroutine WALL

```
      SUBROUTINE WALL(IUNIT,KUNIT,XU,YU,ZU,ZETA,ECZ,ILIN,
     1                IPLAS)
C
C SUBROUTINE WALL MODIFIED FOR ETA RING ANALYSES
C
C
C VARIABLE SHELL WALL PROPERTIES DOWN THE LENGTH OF THE
C RIGHT SRB STARTING AT THE TOP CONE
C
      COMMON/WALLX/JWALL
C
C JUMP TO IUNIT-TH SHELL UNIT
C
      IF(IUNIT.EQ.1)  GO TO  701
      IF(IUNIT.EQ.2)  GO TO  801
      IF(IUNIT.EQ.3)  GO TO  901
      IF(IUNIT.EQ.4)  GO TO  1001
      IF(IUNIT.EQ.5)  GO TO  1101
C
C AFT ATTACH CASE ABOVE ET STUBS (UNIT 1)
C
 701  CONTINUE
      JWALL=7
      IF(XU.GT.47.0.AND.XU.LE.53.0) JWALL=13
      RETURN
C
C SEGMENT BETWEEN ET STUBS (UNIT 2)
C
 801  CONTINUE
      JWALL=8
      RETURN
C
C UPPER ET STUB (UNIT 3)
C
 901  CONTINUE
      JWALL=9
      RETURN
C
C LOWER ET STUB (UNIT 4)
C
1001  CONTINUE
      JWALL=9
      RETURN
C
C AFT ATTACH CASE BELOW ET STUBS (UNIT 5)
C
1101  CONTINUE
      JWALL=7
      IF(XU.GE.57.49) JWALL=13
C
C EXIT
C
      RETURN
      END
```

# Appendix B: User-Written Subroutine USRPT

```
      SUBROUTINE USRPT
C
C GENERATE USER POINTS FOR THE NON-SYMMETRIC AFT ET FLANGES
C
      COMMON/UPI/ IUS1,IUS2,IWALL,ICROSS,NCOLS,NELT,KQUAD
      COMMON/UPF/ XG1,XG2,DANGLE
      COMMON/PIE/DTR,RTD,PI
C
C INITIALIZE SOME VARIABLES
C
      IUVW=111
      IRUVW=111
      ISYS=0
      POW=0.0
      ANG1=32.0
      ANG2=296.0
      RADIUS=72.62+1.6378
      IF(NCOLS.EQ.181) RADIUS=72.6865+1.6378
C     DANGLE=360.0/FLOAT(NCOLS-1)
C
C ET STUB EDGE OF UPPER AFT ET FLANGE
C
      IUPT=0
      IUS=IUS1
      IRS=2
      DO 100 I=1,NCOLS
      ANGLE=(I-1)*DANGLE
      IF(ANGLE.LT.ANG1.OR.ANGLE.GT.ANG2) GO TO 100
      ICS=I
      IUPT=IUPT+1
      CALL NODE(IUPT,IUS,IRS,ICS,0.0,0.0,0.0,0,0,0,0.0)
 100  CONTINUE
C
C OUTSIDE EDGE OF UPPER AFT ET FLANGE
C
      XG=XG1
      DO 200 I=1,NCOLS
      ANGLE=(I-1)*DANGLE
      IF(ANGLE.LT.ANG1.OR.ANGLE.GT.ANG2)    GO TO 200
      IF(ANGLE.GE.ANG1.AND.ANGLE.LT.51.0)   GO TO 110
      IF(ANGLE.GE.51.0.AND.ANGLE.LT.255.0)  GO TO 120
      IF(ANGLE.GE.255.0.AND.ANGLE.LT.262.0) GO TO 130
      IF(ANGLE.GE.262.0.AND.ANGLE.LT.270.0) GO TO 140
      IF(ANGLE.GE.270.0.AND.ANGLE.LT.276.5) GO TO 150
      IF(ANGLE.GE.276.5.AND.ANGLE.LT.283.0) GO TO 160
      IF(ANGLE.GE.283.0.AND.ANGLE.LT.287.5) GO TO 170
      IF(ANGLE.GE.287.5.AND.ANGLE.LE.ANG2)  GO TO 180
C
 110  W=3.19+(7.22-3.19)/(51.0-ANG1)*(ANGLE-ANG1)
      GO TO 190
 120  W=7.22
      GO TO 190
 130  W=7.22+(6.79-7.22)/(262.-255.)*(ANGLE-255.)
      GO TO 190
 140  W=6.79+(5.96-6.79)/(270.-262.)*(ANGLE-262.)
      GO TO 190
 150  W=5.96+(4.98-5.96)/(276.5-270.)*(ANGLE-270.)
      GO TO 190
 160  W=4.98+(3.31-4.98)/(283.-276.5)*(ANGLE-276.5)
      GO TO 190
 170  W=3.31+(2.20-3.31)/(287.5-283.)*(ANGLE-283.)
      GO TO 190
 180  W=2.20+(1.25-2.20)/(ANG2-287.5)*(ANGLE-287.5)
C
 190  CONTINUE
      RBAR=RADIUS+W
      ZG=RBAR*COS(DTR*ANGLE)
      YG=RBAR*SIN(DTR*ANGLE)
      IUPT=IUPT+1
      CALL NODE(IUPT,0,0,0,XG,YG,ZG,IUVW,IRUVW,ISYS,POW)
 200  CONTINUE
C
C ET STUB EDGE OF LOWER AFT ET FLANGE
C
      IUS=IUS2
      IRS=2
      DO 1100 I=1,NCOLS
      ANGLE=(I-1)*DANGLE
      IF(ANGLE.LT.ANG1.OR.ANGLE.GT.ANG2) GO TO 1100
      ICS=I
      IUPT=IUPT+1
      CALL NODE(IUPT,IUS,IRS,ICS,0.0,0.0,0.0,0,0,0,0.0)
1100  CONTINUE
C
C OUTSIDE EDGE OF LOWER AFT ET FLANGE
C
      XG=XG2
      DO 1200 I=1,NCOLS
      ANGLE=(I-1)*DANGLE
      IF(ANGLE.LT.ANG1.OR.ANGLE.GT.ANG2)    GO TO 1200
```

```
      IF(ANGLE.GE.ANG1.AND.ANGLE.LT.51.0)   GO TO 1110
      IF(ANGLE.GE.51.0.AND.ANGLE.LT.255.0)  GO TO 1120
      IF(ANGLE.GE.255.0.AND.ANGLE.LT.262.0) GO TO 1130
      IF(ANGLE.GE.262.0.AND.ANGLE.LT.270.0) GO TO 1140
      IF(ANGLE.GE.270.0.AND.ANGLE.LT.276.5) GO TO 1150
      IF(ANGLE.GE.276.5.AND.ANGLE.LT.283.0) GO TO 1160
      IF(ANGLE.GE.283.0.AND.ANGLE.LT.287.5) GO TO 1170
      IF(ANGLE.GE.287.5.AND.ANGLE.LE.ANG2)  GO TO 1180
C
 1110 W=3.19+(7.22-3.19)/(51.0-ANG1)*(ANGLE-ANG1)
      GO TO 1190
 1120 W=7.22
      GO TO 1190
 1130 W=7.22+(6.79-7.22)/(262.-255.)*(ANGLE-255.)
      GO TO 1190
 1140 W=6.79+(5.96-6.79)/(270.-262.)*(ANGLE-262.)
      GO TO 1190
 1150 W=5.96+(4.98-5.96)/(276.5-270.)*(ANGLE-270.)
      GO TO 1190
 1160 W=4.98+(3.31-4.98)/(283.-276.5)*(ANGLE-276.5)
      GO TO 1190
 1170 W=3.31+(2.20-3.31)/(287.5-283.)*(ANGLE-283.)
      GO TO 1190
 1180 W=2.20+(1.25-2.20)/(ANG2-287.5)*(ANGLE-287.5)
C
 1190  CONTINUE
      RBAR=RADIUS+W
      ZG=RBAR*COS(DTR*ANGLE)
      YG=RBAR*SIN(DTR*ANGLE)
      IUPT=IUPT+1
      CALL NODE(IUPT,0,0,0,XG,YG,ZG,IUVW,IRUVW,ISYS,POW)
 1200  CONTINUE
C
C EXIT
C
      RETURN
      END
```

## Appendix C: User-written Subroutine USRELT

```
      SUBROUTINE USRELT
C
C GENERATE THE CONNECTIVITIES FOR THE AFT ET FLANGES
C
      COMMON/UPI/IUS1,IUS2,IWALL,ICROSS,NCOLS,NELT,KQUAD
C
C INITIALIZE SOME VARIABLES
C
      ZETA=0.0
      ECZ=0.0
      ILIN=0
      IPLAS=0
      INTEG=0
      IPENL=0
      ANG1=32.0
      ANG2=296.0
C     DANGLE=360.0/FLOAT(NCOLS-1)
C     NELT=INT((ANG2-ANG1)/DANGLE)
      IF(KQUAD.EQ.410) KBM=210
      IF(KQUAD.EQ.411) KBM=211
      XSI=0.0
      ECYB=0.0
      ECZB=0.0
C
C MESH FOR UPPER ET FLANGE
C
      DO 100 I=1,NELT
      N1=I
      N2=I+1
      N3=NELT+1+I+1
      N4=NELT+1+I
      CALL QUAD(N1,N2,N3,N4,KQUAD,IWALL,ZETA,ECZ,
     1 ILIN,IPLAS,INTEG,IPENL)
C
C ADD BOLT-ON RING CAPS
C
      NR=N1
      CALL BEAM(N4,N3,NR,KBM,ICROSS,XSI,ECYB,ECZB,ILIN,
     1 IPLAS)
100   CONTINUE
C
C MESH FOR LOWER ET FLANGE
C
      NNUF=2*(NELT+1)
      DO 1100 I=1,NELT
      N1=I+NNUF
      N2=I+1+NNUF
      N3=NELT+1+I+1+NNUF
      N4=NELT+1+I+NNUF
      CALL QUAD(N1,N2,N3,N4,KQUAD,IWALL,ZETA,ECZ,
     1 ILIN,IPLAS,INTEG,IPENL)
C
C ADD BOLT-ON RING CAPS
C
      NR=N1
      CALL BEAM(N4,N3,NR,KBM,ICROSS,XSI,ECYB,ECZB,ILIN,
     1 IPLAS)
C
1100  CONTINUE
C
C EXIT
C
      RETURN
      END
```

# Appendix D: Example STAGSC-1 Input Data

```
ETA RING BASELINE MODEL OF RIGHT SRB  $A-1
C
C EQUIVALENT SHELL MODEL OF FIELD AND FACTORY JOINTS
C MODEL GOES FROM FORWARD CONE TO THE AFT SKIRT
C VARIATION IN SHELL WALL PROPERTIES MODELED
C USING SUBROUTINE WALL TO PICK THE WALL TABLE
C NUMBER FROM THE K-CARDS
C
C ASYMMETRIC ET FLANGES MODELED AS ELEMENT UNIT USING
C SUBROUTINES USRPT AND USRELT
C
3  1  1  0  0  0  1  0  $B-1
5  1  0  9  $B-2
3  9  14 1 $B-3
0.2  0.2  1.0  $C-1  LOAD FACTORS
0  14400  10  10  -1  $D-1
C
C MESH DISCRETIZATION
C
14 46,  $F-1  SEGMENT ABOVE AFT ET RINGS UNIT 1
 3 46,  $F-1  SEGMENT BETWEEN AFT ET RINGS UNIT 2
 2 46,  $F-1  UPPER AFT ET STUB RING UNIT 3
 2 46,  $F-1  LOWER AFT ET STUB RING UNIT 4
12 46   $F-1  SEGMENT BELOW AFT ET RINGS UNIT 5
C
C SHELL UNIT CONNECTION AND CLOSURE CARDS
C
1  2  1  4  $G-1 SEGMENT ABOVE AFT ET STUBS CLOSURE
1  3  2  1  $G-1
1  3  3  1  $G-1
2  2  2  4  $G-1 SEGMENT BETWEEN AFT ET STUBS CLOSURE
2  3  4  1  $G-1
2  3  5  1  $G-1
3  2  3  4  $G-1 UPPER AFT ET STUB CLOSURE
4  2  4  4  $G-1 LOWER AFT ET STUB CLOSURE
5  2  5  4  $G-1 SEGMENT BELOW AFT ET STUBS CLOSURE
C
C USER WRITTEN ROUTINES FOR USRELT,USRPT, AND WALL
C
0  0  0  0  0  1  1  $H-1
C
C D6AC STEEL PROPERTIES
C
1  $I-1
30.0E+6  0.3  0.0  0.283  $I-2
C
C ALUMINIUM PROPERTIES
C
2  $I-2
10.0E+6 0.3  0.0  0.102  $I-2
C
C DUMMY MATERIAL PROPERTIES
C
3  $I-2
0.1E+6 0.0  0.0  0.102  $I-2
C
C TABLE OF RING AND STRINGER PROPERTIES FOLLOWS
C
C
C FWD ET/SRB LOAD INTRO RING
C
1  1  1  0  2000.  0.  0.$J-1
10.  1000.  1000.  0.$J-2A
C
C ET FLANGE BOLT-ON RING CAPS
C
2  1  1  0  1.91178  0.0  0.0  $J-1
1.79  0.477945  0.149167  0.0  $J-2A
C
C STUB RINGS
C
3  1  1  0  0.0542  0.0  0.0  $J-1
0.34  0.0524  0.0018  0.0  $J-2A
C
C T-SHAPED RING PROPERTIES
C
4  1  1  0  3.5551  0.0  0.0  $J-1
1.5298  2.8355  0.7196  0.0  $J-2A
C
C AFT DOME BOSS RING
C
5  1  1  0  9.5319  0.0  0.0  $J-1
7.5625  4.766  4.766  0.0  $J-2A
C
C AFT CONICAL SKIRT RINGS
C
6  1  2  0  2000.  0.  0.$J-1
10.  1000.  1000.  0.$J-2A
C
C AFT CONICAL SKIRT STRINGERS
```

```
C
7  1  2  0  .0521  0.  0.$J-1
.5  .0417  .0104  0.$J-2A
C
C AFT HOLD-DOWN POSTS
C
8  1  2  0  2000.  0.  0.$J-1
10.  1000.  1000.  0.$J-2A
C
C FWD ET/SRB LOAD INTRO SIDE RINGS
C
9  1  3  0  2000.  0.  0.$J-1
10.  1000.  1000.  0.$J-2A
C
C SHELL WALL DEFINITIONS
C
1  1  1  $K-1 FORWARD CONE
1  0.5  $K-2
2  1  1  $K-1  FORWARD SKIRT
1  0.5  $K-2
3  1  1  $K-1 FORWARD DOME
1  0.5  $K-2
4  1  1  $K-1  FORWARD CASE
1  0.5  $K-2
5  1  1  $K-1  FORWARD CENTER CASE
1  0.5  $K-2
6  1  1  $K-1  AFT CENTER CASE
1  0.5  $K-2
7  1  1  $K-1  AFT ATTACH CASE ABOVE AND BELOW AFT ET RINGS
1  0.6  $K-2
8  1  1  $K-1  BETWEEN ET RINGS
1  0.62  $K-2
9  1  1  $K-1  AFT ET STUBS
1  0.4  $K-2
10  1  1 $K-1  AFT ATTACH CASE AND AFT SKIRT CYLINDER
1  0.56  $K-2
11  1  1 $K-1  AFT DOME
1  0.362 $K-2
12  1  1 $K-1  AFT SKIRT CONE
2  0.50  $K-2
13 1  3  $K-1  TANG/CLEVIS EQUIVALENT SHELL WALL
1  0.300 $K-2  INNER CLEVIS LUG
1  0.500 $K-2  TANG
1  0.300 $K-2  OUTER CLEVIS LUG
14  1  1 $K-1  AFT ET FLANGES
1  0.25  $K-2
C
C USER PARAMETERS
C
8  10  $L-1
C
C ET STUB SHELL UNIT NUMBERS,WALL TABLE FOR FLANGES,RING CAP
C TABLE, NUMBER OF COLUMNS, NUMBER OF FLANGE ELEMENTS, KQUAD
C NUMBER OF USER POINTS DEFINED ON CARDS
C
C  IUS1,IUS2,IWALL,ICROSS,NCOLS,NELT,KQUAD,NPTS
3  4  14  2  46  33  411 0  $L-2A
C
C GLOBAL AXIAL LOCATION OF ET STUBS RINGS AND
C   CIRCUMFERENTIAL ANGLE PER FLANGE ELEMENT
C
63.54  75.51  8.0,  $L-2B  XG1,XG2,DANGLE
C
C   P(1) TO P(7) SRM PRESSURE DIST.
C
988. 926. 910. 893. 887. 893. 907.  $L-2B
C
C*****************************************************
C
C SHELL UNIT DEFINITIONS
C
C*****************************************************
C
C AFT ATTACH CASE FROM 1491 TO 1505 (UNIT 1)
C SEGMENT ABOVE AFT ET RINGS
C
5  0  $M-1
0.0  63.54  0.0  360.0  72.62  $M-2A  CYLINDER
0  $M-5  SHELL WALL TYPE
411  3  $N-1 ELEMENT TYPE
47.0 6.0 10.54  $N-2
 9   2     2   $N-3
0 6 6 6   $P-1
111  100  $P-2
1  $Q-1
1  1  $Q-2
1000.0  5  3  0  0  $Q-3  LIVE PRESSURE
1  1  0  0  0  1  $R-1
C
C SEGMENT BETWEEN ET ATTACHMENT FLANGES (UNIT 2)
C
5  1  $M-1  CYLINDRICAL PANEL
```

```
183 0.0  11.97  0.0  360.0  72.62  $M-2A
184 0  0  0.0  0.02  $M-5 SELECT WALL TYPE AND SET ECCENTRICITY
185 411  $M-1  SELECT ELEMENT TYPE
186 6  6  6  6  $P-1  BOUNDARY CONDITIONS
187 1  $Q-1  LOADS
188 1  1  $Q-2
189 1000.0  5  3  0  0  $  LIVE PRESSURE LOADING
190 1  1  0  0  0  1  $R-1  PRINT OPTIONS
191 C
192 C UPPER ET ATTACHMENT FLANGE (UNIT 3)
193 C
194 4  1  $M-1  ANNULAR PLATE
195 72.62  74.2578  0.0  360.0  $M-2A
196 0  $M-5  SELECT WALL TYPE
197 411  $M-1  SELECT ELEMENT TYPE
198 6  6  3  6  $P-1  BOUNDARY CONDITIONS
199 0  $Q-1  LOADS
200 1  1  0  0  0  1  $R-1  PRINT OPTIONS
201 C
202 C LOWER ET ATTACHMENT FLANGE (UNIT 4)
203 C
204 4  1  $M-1  ANNULAR PLATE
205 72.62  74.2578  0.0 360.0  $M-2A
206 4  $M-5  SELECT WALL TYPE
207 411  $M-1  SELECT ELEMENT TYPE
208 6  6  3  6  $P-1  BOUNDARY CONDITIONS
209 0  $Q-1  NO LOADS
210 1  1  0  0  0  1  $R-1  PRINT OPTIONS
211 C
212 C SEGMENT BELOW AFT ET RING FROM 1517 TO 1577 (UNIT 5)
213 C FACTORY JOINT AT 1577
214 C
215 5  1  $M-1
216 0.0  60.49  0.0  360.0  72.62  $M-2A  CYLINDER
217 0  $M-5  SHELL WALL MODEL
218 411  2  $N-1  ELEMENT TYPE
219 57.49  3.0  $N-2
220  10     1   $N-3
221 6 6 0 6     $P-1
222 001  010  $P-2
223 1  $Q-1
224 1  1  $Q-2
225 1000.0  5  3  0  0  $Q-3  LIVE PRESSURE
226 1  1  0  0  0  1  $R-1
227 C
228 C ELEMENT UNIT DATA
229 C
230 1  $U-1
231 1  8  $U-2
232 C STRUT LOADS FOR TOP ET FLANGE
233 0.0  1  3  59  0  1  $Q-3  0.5 * P8
234 0.0  1  3  48  0  1  $Q-3  0.5 * P9
235 0.0  1  2  55  0  1  $Q-3  0.5 * P10 IN Yg DIRECTION
236 0.0  1  3  55  0  1  $Q-3  0.5 * P10 IN Zg DIRECTION
237 C STRUT LOADS FOR BOTTOM ET FLANGE
238 0.0  1  3  127  0  1  $Q-3  0.5 * P8
239 0.0  1  3  116  0  1  $Q-3  0.5 * P9
240 0.0  1  2  123  0  1  $Q-3  0.5 * P10 IN Yg DIRECTION
241 0.0  1  3  123  0  1  $Q-3  0.5 * P10 IN Zg DIRECTION
242 1  1  0  0  0  1  $V-1
```

NASA
National Aeronautics and Space Administration

# Report Documentation Page

| 1. Report No. | 2. Government Accession No. | 3. Recipient's Catalog No. |
|---|---|---|
| NASA TM-89164 | | |

| 4. Title and Subtitle | 5. Report Date |
|---|---|
| Nonlinear Shell Analyses of the SRB/ETA Ring Interface | July 1987 |
| | 6. Performing Organization Code |

| 7. Author(s) | 8. Performing Organization Report No. |
|---|---|
| Norman F. Knight, Jr. | |
| | 10. Work Unit No. 554-14-21-50 |

| 9. Performing Organization Name and Address | 11. Contract or Grant No. |
|---|---|
| NASA Langley Research Center<br>Hampton, VA 23665-5225 | |
| | 13. Type of Report and Period Covered<br>Technical Memorandum |

| 12. Sponsoring Agency Name and Address | 14. Sponsoring Agency Code |
|---|---|
| National Aeronautics and Space Administration<br>Washington, DC 20546-0001 | |

15. Supplementary Notes

16. Abstract

Two-dimensional shell models of the portion of the solid rocket booster (SRB) with the external tank attachment (ETA) ring have been developed using the STAGSC-1 computer code. These analyses have been performed in support of the SRB recertification program underway at the NASA Marshall Space Flight Center The purpose of these analyses is to calculate the overall stress and deflection distributions for the SRB/ETA ring interface. An overview of the SRB/ETA ring geometry is presented followed by a discussion of the analysis methods and finite element models. Finally, the nonlinear structural response of the SRB/ETA ring interface is discussed.

| 17. Key Words (Suggested by Author(s)) | 18. Distribution Statement |
|---|---|
| Solid Rocket Booster<br>External Tank Attachment Ring<br>Space Shuttle<br>Structural Analysis<br>STAGS | Unclassified - Unlimited<br><br>Subject Category 39 |

| 19. Security Classif. (of this report) | 20. Security Classif. (of this page) | 21. No. of pages | 22. Price |
|---|---|---|---|
| Unclassified | Unclassified | 62 | A04 |

NASA FORM 1626 OCT 86